Consistent quadrupole-octupole collective model

A. Dobrowolski,[1,*] K. Mazurek,[2,†] and A. Góźdź[1,‡]

[1]*Department of Theoretical Physics, Maria Curie-Skłodowska University, pl. Marii Curie-Skłodowskiej 1, PL-20031 Lublin, Poland*
[2]*Institute of Nuclear Physics PAN, ul. Radzikowskiego 152, Pl-31342 Kraków, Poland*

Within this work we present a consistent approach to quadrupole-octupole collective vibrations coupled with the rotational motion. A realistic collective Hamiltonian with variable mass-parameter tensor and potential obtained through the macroscopic-microscopic Strutinsky-like method with particle-number-projected BCS (Bardeen–Cooper–Schrieffer) approach in full vibrational and rotational, nine-dimensional collective space is diagonalized in the basis of projected harmonic oscillator eigensolutions. This orthogonal basis of zero-, one-, two-, and three-phonon oscillator-like functions in vibrational part, coupled with the corresponding Wigner function is, in addition, symmetrized with respect to the so-called symmetrization group, appropriate to the collective space of the model. In the present model it is D_4 group acting in the body-fixed frame. This symmetrization procedure is applied in order to provide the uniqueness of the Hamiltonian eigensolutions with respect to the laboratory coordinate system. The symmetrization is obtained using the projection onto the irreducible representation technique. The model generates the quadrupole ground-state spectrum as well as the lowest negative-parity spectrum in ^{156}Gd nucleus. The interband and intraband $B(E1)$ and $B(E2)$ reduced transition probabilities are also calculated within those bands and compared with the recent experimental results for this nucleus. Such a collective approach is helpful in searching for the fingerprints of the possible high-rank symmetries (e.g., octahedral and tetrahedral) in nuclear collective bands.

I. INTRODUCTION

The concept of the shape of the nucleus has existed since the beginning of the theory of the atomic nucleus, even if, on many points, it stays in contradiction to the well-established concepts of quantum mechanics. The verification of the deformation of nuclear surface is done mainly by investigating the behavior of experimental observables such as rotational spectra of quadrupole or octupole deformed nuclei [1,2], the transition probabilities, magnetic moments, and some properties of K isomers [3,4]. In this paper we focus our attention mainly on the low-energy quadrupole and octupole shape vibrations as the results of collective coherent motions of substantial number of nucleons.

There are few articles speaking about a possibility of existing the nonaxial octupole stable configurations, i.e., Refs. [5–9]. The problem of nuclear shape vibrations has been investigated by several authors in Refs. [10,11], using the Bohr Hamiltonian [12–14], the Interacting Boson Model (IBM) [15,16], or the analytic collective model (AQOA) [17]. Also the new approach based on cluster Hamiltonian are shown in Ref. [18]. The main issue of all those approaches is to search for stable nuclear configurations as well as the strengths of electromagnetic transitions between collective states. The quadrupole and octupole deformation parameters are usually treated as collective variables.

The approach proposed in the present paper assumes that the shape of the collective potential included in the collective Hamiltonian is obtained within the so-called macroscopic-microscopic total energy calculations using the Strutinsky method with the Woods-Saxon mean field [7,19].

The nuclear surface is described in terms of spherical harmonics, limited to the dipole ($\lambda = 1$), quadrupole ($\lambda = 2$), and octupole ($\lambda = 3$) parts. This shape parametrization offers a series of advantages in certain nuclear structure theory developments. For the present study, it enables exact treatment of the uniqueness of quantum solutions transformed from the laboratory to the intrinsic (body fixed) reference frame.

However, this problem is well fixed for the pure quadrupole shape vibrations in the textbooks (see, e.g., Ref. [20]), and it requires significant modifications if only some vibrational modes, selected from among a full set of octupole degrees of freedom, are switched on. The detailed study of chosen modes in terms of the *intrinsic symmetry-group-theory* formalism [21], known as the determination of the *symmetrization group,* is presented in Ref. [22] and references therein. The formalism of the intrinsic group allows us to unambiguously determine the *minimal* subdomain of the intrinsic collective manifold (cf. deformation parameters and Euler angles) in which the transformation of wave functions and physical operators between the intrinsic and laboratory frame is one to one. The collective Hamiltonian is diagonalized in the space of symmetrized basis functions. This permits us to calculate the reduced probabilities of electric dipole and quadrupole transitions. The systematic knowledge of electromagnetic-reduced transition probabilities $B(E\lambda)$ is essential to discover a possibility of existing the high-rank symmetries of collective states which has not been yet widely discussed. A symmetry, among other physical effects, is a crucial factor determining the structure of wave functions and thus strongly affects the transition probabilities $B(E\lambda)$.

---
*arturd@kft.umcs.lublin.pl
†Katarzyna.Mazurek@IFJ.edu.pl
‡Andrzej.Gozdz@umcs.lublin.pl

The paper is organized as follows: Section II gives the details of the nuclear shape parametrization. Section III defines the conditions for the uniqueness of intrinsic Hamiltonian eigensolutions in the laboratory frame. In Sec. IV we define the vibrational part of a collective Hamiltonian. Section V is devoted to construction of the so-called generalized rotor Hamiltonian which is a part of the total Hamiltonian. The generalization consists in using in its construction the angular-momentum operators in powers higher than two. This allows for obtaining higher than dihedral (D_2) symmetries of nonaxial rotor. In Sec. V A we construct the basis for a diagonalization of the full Hamiltonian. The aim of Sec. VI is to show the importance of the center-of-mass motion generated by the octupole modes and connected with this induced dipole deformations. In Secs. VII and VII B we give details of the collective potential construction as well as several examples of its two-dimensional cuts. Finally, in Sec. VIII we calculate the $B(E1)$ and $B(E2)$ reduced transition probabilities for the ground-state and the lowest-negative-parity bands with the presence of octupole vibrations.

II. COLLECTIVE QUADRUPOLE-OCTUPOLE SPACE IN INTRINSIC FRAME

Since our efforts are mainly focused on an investigation of the possibility of existing spatial symmetries possessing two- and three-dimensional irreducible representations, the intrinsic collective variables are chosen to be the components of the irreducible tensor $\alpha_{\lambda\mu}$. This tensor has well-defined properties with regard to the group-theory formalism. The latter allows us to describe the shape of the nuclear surface in the body-fixed reference frame within standard multipole expansion of $\{\theta,\varphi\}$ angles.

The main goal is to expand the nuclear surface in the intrinsic reference frame in terms of the orthogonal basis set of the spherical harmonics $\{Y_{\lambda\mu}\}$, which are also spherical tensors,

$$R(\vartheta,\varphi) = R_0 c(\alpha)\left[1 + \sum_{\lambda=1}^{\lambda_{\max}}\sum_{\mu=-\lambda}^{\lambda}(\alpha_{\lambda\mu}^{\star})Y_{\lambda\mu}(\vartheta,\varphi)\right], \quad (1)$$

where $\alpha \equiv \{\alpha_{\lambda\mu}\}$ and the function $c(\alpha)$ are obtained from the nuclear volume conservation condition. As shown in Sec. VI, the dipole α_{10} and $\alpha_{1\pm1}$ variables, determined from the condition that the center of mass of the nuclear body is fixed in the beginning of the coordinate system, are dependent on $\{\alpha_{2\nu},\alpha_{3\mu}\}$ variables.

Let us keep in mind that for any spherical tensor defined in the SO(3) manifold, the following relation is true:

$$\alpha_{\lambda\mu}^{\star} = (-1)^{\nu}\alpha_{\lambda-\mu}. \quad (2)$$

Such an expansion, reproducing an infinite number of physically important nuclear shapes, has been successfully used for a long time, e.g., in Refs. [23–25].

Since the collective space spanned by two quadrupole variables, $\alpha_{20}, \alpha_{22} = \alpha_{2-2}$, with the three conditions

$$\alpha_{21} = \alpha_{2-1} = 0, \quad (3)$$

determines a body-fixed frame, the full octupole $\{\alpha_{3\nu}\}, \nu = 0,1,2,3$ complex tensor together with Euler angles from the 12-dimensional collective-variable space. Obviously, this is not the principal axes frame but it allows for using the traditional picture of quadrupole collective motion. The determination of the Hamiltonian matrix elements or any physical constituents, with a reasonable accuracy, makes a problem quite serious in such a multidimensional space. In order to efficiently deal, e.g., with time-consuming multidimensional integrals and, at the same time, investigate effective contributions from all octupole modes, one can lower the dimensionality of space by putting all $\{\alpha_{3\nu}\}$ to be *real* numbers. This implies, by virtue of Eq. (2), that $\alpha_{3\mu}$ and $\alpha_{3-\mu}$ are mutually dependent, which obviously leads to the reduction of dimensionality of the model to nine dimensions (including Euler angles). As it turns out, the calculations of desired matrix elements within the space of Euler angles can be done totally analytically. Finally, the independent collective variables used in the present study are $(\alpha_{20},\alpha_{22},\{\text{Re}(\alpha_{3\nu})\})$ with ν index running over the positive integers only, i.e., $\nu = \{0,1,2,3\}$, describing the axial, nonaxial quadrupole vibrational modes and the four real octupole modes, respectively. Now, we can rewrite Eq. (1) to the following form:

$$R(\vartheta,\varphi) = R_0 c(\alpha)\left[1 + \alpha_{10}Y_{10}(\vartheta,\varphi) + \alpha_{20}Y_{20}(\vartheta,\varphi)2\right.$$
$$+ \alpha_{11}\text{Re}(Y_{11}(\vartheta,\varphi)) + 2\alpha_{22}\text{Re}(Y_{22}(\vartheta,\varphi))$$
$$\left. + \alpha_{30}Y_{30}(\vartheta,\varphi) + 2\sum_{\mu=1}^{3}\alpha_{3\mu}\text{Re}(Y_{3\mu}(\vartheta,\varphi))\right]. \quad (4)$$

One should realize that the price for such a reduction of collective space is the appearance of three additional to Eq. (3) conditions on the $\alpha_{3\mu}$ tensor

$$\text{Im}(\alpha_{3\mu}) = 0, \quad (5)$$

which should be conserved during the collective motion. Conditions (5) together with (3) imply that the differentials of the scalars of β_{λ}^2 type for both the quadrupole ($\lambda = 2$) and octupole ($\lambda = 3$) collective spaces can be written as $d\beta_2^2 = d\alpha_{20}^2 + 2d\alpha_{22}^2$ and $d\beta_3^2 = d\alpha_{30}^2 + 2d\alpha_{31}^2 + 2d\alpha_{32}^2 + 2d\alpha_{33}^2$. Therefore, the metric tensors associated with these quadrupole and octupole spaces are given, respectively, as $g_{\nu\nu}^{(2)} = \text{diag}(1,2)$ and $g_{\mu\mu}^{(3)} = \text{diag}(1,2,2,2)$.

III. UNIQUENESS OF PHYSICAL STATES

In this section we address the problem of the uniqueness of collective eigensolutions in the laboratory coordinate system in which a nucleus is observed and measured. The vibrational-rotational collective approach presented here, because of the particular choice of collective variables, defines the collective Hamiltonian and thus also its eigensolutions in the body-fixed frame.

The transformation from the intrinsic to the laboratory frame is necessary to calculate, for example, the reduced transition probabilities. However, due to conditions (3) and (5) imposed onto the intrinsic quadrupole $\alpha_{2\nu}$ and octupole

$\alpha_{3\mu}$ variables, respectively, such a transformation turns out to be generally not reversible and, by consequence, not unique. In what follows, we show the method, based on the intrinsic group formalism, that ensures this uniqueness. This method is called *symmetrization*.

A. Intrinsic groups

As we have already mentioned, with regard to conditions (3) and (5), the vibrational-rotational Hamiltonian, its eigenvectors, and other quantum observables should be symmetrized, since they are all the function of quadrupole and octupole variables. In other words, they have to be invariant with respect to the symmetrization group of the model, $\bar{G}_s$. As shown in Ref. [22], in the case of $(\alpha_{20}, \alpha_{22}, \{a_{3\nu}\})$, $\nu = \{0,1,2,3\}$ space, this *intrinsic* group acting in the body-fixed frame is formed by the following eight symmetry operations (proper rotations) $\bar{g}$: $\{I, C_{2x}, C_{2y}, C_{2z}, C_{4y}, C_{4y}^{-1}, C_{2c}, C_{2d}\}$, where C_{ni} denotes the rotation about the body-fixed axis marked with index i by the $2\pi/n$ angle and I is the unity operation. The axes c and d are skew with respect to the OX, OY, OZ axes, see Ref. [26]. Such a set of transformations is recognized as the D_4 group with the main OY axis. This group is a subgroup of the already-mentioned octahedral group O_h.

Studying any transformation $\bar{g}$ of an object defined in the body-fixed frame, we should remember that its axes move together with the object, contrary to the transformations in the laboratory frame, where the coordinate system axes are fixed in the space. It implies that the intrinsic transformations act on both the $\alpha_{\lambda\mu}$ variables and Euler angles Ω, keeping the body untouched in the laboratory system. Mathematically, such action of an arbitrary rotation $\bar{g}$ belonging to the intrinsic group, $\bar{g} \in S\bar{O}(3)$ is given as:

$$\left(\alpha_{\lambda\mu}^{\text{lab}}\right)' = \bar{g}\alpha_{\lambda\mu}^{\text{lab}} = \alpha_{\lambda\mu}^{\text{lab}}, \tag{6}$$

$$\left(\alpha_{\lambda\mu}\right)' = \bar{g}\alpha_{\lambda\mu} = \sum_{\mu'} D_{\mu'\mu}^{\lambda}(g^{-1})\alpha_{\lambda\mu'}, \tag{7}$$

$$\Omega' = \bar{g}\Omega = \Omega g. \tag{8}$$

In the function space of intrinsic variables $\alpha_{\lambda\mu}$ and Euler angles Ω, any action $\bar{g}$ is performed in the following way:

$$\bar{g}\psi(\alpha_{\lambda\mu}, \Omega) = \psi(\bar{g}\alpha_{\lambda\mu}, \bar{g}^{-1}\Omega),$$
$$\bar{g}\,R_{\text{MK}}^{J}(\Omega) = R_{\text{MK}}^{J}(\Omega g^{-1})$$
$$= \sqrt{2J+1}\sum_{K=-J}^{J} D_{\kappa K}^{J}(g)\,D_{\text{MK}}^{J*}(\Omega), \tag{9}$$

where $R_{\text{MK}}^{J}(\Omega) \equiv \sqrt{2J+1}\,D_{\text{MK}}^{J*}(\Omega)$ denote the standard normalized complex conjugated set of Wigner functions playing usually a role of basis states to diagonalize the rotational Hamiltonians defined in the intrinsic frame [27].

Since the formalism of intrinsic groups is not widely applied, let us introduce some of its formal properties as proposed in Ref. [21].

Let $\mathcal{L}_G$ be a linear space containing all possible vectors S_G obtained as formal sums of the elements g of the group G with

the combination coefficients $c(g) \in C$,

$$S_G = \sum_{g \in G} c(g)g. \tag{10}$$

The addition and multiplication group operations are defined adequately to the nature of the group elements. The elements of the intrinsic group $\bar{G}$ induced by G is regarded as the collection of operators $\bar{g}$ which act on elements $S_G \in \mathcal{L}_G$ in the following way:

$$\forall S_G \in \mathcal{L}_G, \quad \bar{g}S_G = S_G g. \tag{11}$$

The elements $\bar{g}$ of the intrinsic group are scalars with respect to operations $g \in G$. It implies that the action $\bar{g} \in \bar{G}$ does not affect the tensor objects defined in G [see the first equation in Eq. (8)]. The latter is equivalent to the fact that the intrinsic and laboratory frames are independent; the operations from the intrinsic and laboratory groups commute, i.e., $[\bar{G}, G] = 0$.

The groups $\bar{G}$ and G are anti-isomorphic, i.e., there exists the one-to-one correspondence $\phi_G : \bar{G} \rightarrow G$ satisfying, for all $\bar{g} \in \bar{G}$, the relation

$$\phi_G(\bar{g}) = g,$$
$$\phi_G(\bar{g}_1\bar{g}_2) = g_2\,g_1. \tag{12}$$

The last property of Eq. (12) defines the superposition pattern of intrinsic group elements which turns to be opposite with respect to the elements of G. It allows us, in addition, to apply the already-known properties of the laboratory group, as irreducible representations, Clebsch-Gordan coupling coefficients, and others to the corresponding intrinsic groups. The above overall consideration leads also to the generalization of the well-known fact that the commutation relations between the angular-momentum operators expressed in the laboratory and body-fixed frames have opposite signs, see, for example, Ref. [28].

B. Symmetrization procedure

Since physical observables, particularly the reduced transition probabilities which we are interested in here, are measured with respect to the laboratory coordinate system, we have to define the relation between the tensor operators $\hat{T}_{\lambda\mu}^{\text{lab}}$ and $\hat{\bar{T}}_{\lambda\mu}$ expressed in laboratory and intrinsic frames, respectively:

$$\hat{T}_{\lambda\mu}^{\text{lab}} = \sum_{\nu=-\lambda}^{\lambda} D_{\mu\nu}^{\lambda*}(\Omega)\hat{\bar{T}}_{\lambda\nu}. \tag{13}$$

If the above is used for collective variables of nuclear shape, i.e., $\hat{T}_{\lambda\mu} \equiv \alpha_{\lambda\mu}$, then it reads

$$\alpha_{\lambda\mu}^{\text{lab}} = \sum_{\nu=-\lambda}^{\lambda} D_{\mu\nu}^{\lambda*}(\Omega)\bar{\alpha}_{\lambda\nu}$$
$$f_k(\alpha_{\lambda\mu}, \Omega) = 0, \quad \{k = 1, 2, \ldots N_f\}, \tag{14}$$

where f_k are the additional conditions imposed on the intrinsic variables while N_f is the number of all conditions defining a model of collective variables. Among those conditions, three of them should determine the orientation of both intrinsic versus laboratory frame or, in other words, Euler angles Ω.

In the presence of the conditions $\{f_k\}$, the transformation (14) is, in general, nonreversible. It means that, for one given set of laboratory variables, $\{\alpha_{\lambda\nu}^{\text{lab}}\}$ usually may correspond to several sets of intrinsic variables $\{\bar{\alpha}_{\lambda\mu}, \Omega\}$. Since, by virtue of Eq. (14), any $\alpha_{\lambda\nu}^{\text{lab}}$ is a function of the set $\{(\bar{\alpha}_{\lambda\mu}, \Omega)\}$, it may happen that

$$\alpha_{\lambda\nu}^{\text{lab}}(\{\alpha_{\lambda\mu}, \Omega\}) = \alpha_{\lambda\nu}^{\text{lab}}(\{\alpha'_{\lambda\mu}, \Omega'\}), \qquad (15)$$

where, by definition, $(\{\alpha_{\lambda\mu}, \Omega\}) \neq (\{\alpha'_{\lambda\mu}, \Omega'\})$.

One can therefore conclude that there may exist several subdomains of intrinsic $\alpha_{\lambda\mu}$ space which produce the same nuclear shapes but they are, however, rotated with respect to the laboratory coordinate system. Such a feature of $\bar{\alpha}$-type variables has its consequences for the eigensolutions of the collective Hamiltonians breaking the uniqueness, one of the fundamental properties of the physical solution in the laboratory frame. Traditionally, in order to restore the above-mentioned uniqueness of quantum solutions, one first must find a kind of "minimal subdomain" of intrinsic α's which, by multiple applying all transformations of a given intrinsic group, fully covers the entire domain. The intrinsic symmetry group of those properties is referred to as *symmetrization group* $\bar{G}_s$. All the transformations $\bar{g}$ of this group should satisfy the condition

$$\alpha_{\lambda\nu}^{\text{lab}}(\bar{g}\alpha_{\lambda\nu}, \bar{g}^{-1}\Omega)) = \alpha_{\lambda\nu}^{\text{lab}}(\alpha_{\lambda\nu}, \Omega). \qquad (16)$$

This group has been already found for the ensemble of $(\{\alpha_{2\nu}\}, \{\alpha_{3\mu}\}, \{\Omega\})$ with various conditions f_k introduced in Eq. (14). For a detailed study of the symmetrization problem, see Refs. [29–32]. The symmetrization condition for collective states, say, $\Psi(\alpha, \Omega)$, comes directly from properties (8) and (15), namely requiring that $\Psi(\alpha, \Omega) = \Psi(\alpha', \Omega')$ and $\Psi(\alpha', \Omega') = \Psi(\bar{g}\alpha, \bar{g}^{-1}\Omega)$, and we conclude by means of Eq. (9) that for all $\bar{g} \in \bar{G}_s$

$$\bar{g}\Psi(\alpha, \Omega) = +1\Psi(\alpha, \Omega). \qquad (17)$$

The relation (17), rendering the uniqueness of quantum solutions in the laboratory frame, says that each quantum state as the eigensolution of the collective Hamiltonian should necessarily be invariant with regard to the scalar representation of the $\bar{G}_s$ symmetrization group.

One should, however, clearly distinguish between the symmetry group of the intrinsic Hamiltonian, as it is usually associated with the shape of the nuclear body and the symmetrization group $\bar{G}_s$. Each of those two types of groups influences different aspects of the collective model. As we remember, in the Bohr Hamiltonian model, the vibrational and rotational sub-Hamiltonians are octahedrally $\bar{O}_h$ invariant in the intrinsic frame. This, of course, is not the only symmetry group of possible transformations of which the Hamiltonian is invariant. The full symmetry of the Hamiltonian is discussed in a more formal way in Ref. [33].

If, for example, one wishes to transform the SO(3)-symmetric laboratory Hamiltonian of a five-dimensional harmonic oscillator to the intrinsic coordinates, the transformation (14) should be applied. The latter reduces the number of independent intrinsic vibrational variables due to the accompanying additional conditions. By consequence, the laboratory symmetry SO(3) of the laboratory Hamiltonian reduces to

the intrinsic octahedral symmetry which only accidentally is identical to the symmetrization group. In this context, the symmetrization group $\bar{G}_s$ can be treated as the *maximal* symmetry group of the Hamiltonian, which is possible to be constructed out of the actual intrinsic variables of α and Ω type and transforming all of them at the same time. On the other hand, the latter may be treated as the set of transformations which have to be satisfied to allow the intrinsic Hamiltonian eigensolutions to be interpreted as physical solutions in the laboratory frame.

IV. QUADRUPOLE + OCTUPOLE COLLECTIVE HAMILTONIAN

A traditional way of constructing a consistent vibrational-rotational collective approaches accounts on defining the collective Hamiltonian with respect to the laboratory coordinate system using the laboratory collective variables, e.g., $\alpha_{\lambda\mu}^{\text{lab}}$ and, next, transforming it to the body-fixed frame. A standard kinetic energy term in the well-known Bohr Hamiltonian approach (see Ref. [12] and references therein), which is obtained from a simple five-dimensional harmonic-oscillator Hamiltonian in $\alpha_{2\mu}^{\text{lab}}, \mu = \{-2, -1, 0, 1, 2\}$ variables transformed to the intrinsic frame, scatters out into four terms. Three of these terms correspond to the energy of surface vibrations towards the quadrupole β and γ modes while the fourth one describe the rotational energy of the body expressed in terms of Euler angles.

The procedure according to this scheme, i.e., starting from the 12-dimensional quadrupole-octupole laboratory Hamiltonian, was a subject of studies presented in Ref. [34] which results in a consistent form of quadrupole-octupole collective Hamiltonian in the body-fixed frame. Such a Hamiltonian, unfortunately, cannot be efficiently applied in practice. A similar study but for pure octupole degrees of freedom has been done in Ref. [35].

Contrarily to the above-outlined concept, we construct the collective vibrational-rotational Hamiltonian already in the intrinsic frame applying the so-called *adiabatic approximation*, which allows the separation of the vibrational and rotational motions. Such separation is, in general, possible due to substantially different (by 2–3 orders of magnitude) energy scales of both the vibrational and rotational collective modes.

We therefore propose, to some extent, an even more simplified approach in which quadrupole and octupole vibrational modes are totally decoupled in the kinetic-energy term. Such an approximation seems to be justified since the values of the mass-tensor components, responsible for this coupling, are, on average, about one order of magnitude smaller than the smallest value of the octupole mass-tensor components in the vicinity of the ground-state point.

The full six-dimensional vibrational collective space, as defined in Sec. II, for the mass parameter functions can be then treated as the tensor product of the quadrupole two-dimensional and octupole four-dimensional subspaces. This allows for evaluating the quadrupole and octupole kinetic-energy terms independently.

Let us recall that, in general, the quadrupole-octupole coupling mass tensor components are, in general, functions of all six collective variables $\{\alpha_{2\nu}, \alpha_{3\mu}\}$. Neglecting this coupling, we determine two independent mass tensors: first, for pure quadrupole motion admitting that the octupole deformation is fixed to zero and, second, corresponding to the octupole motion, for which the quadrupole configuration corresponds to the ground-state point. Such approximations make the calculations of the mass tensor feasible, accelerating numerical calculations by a factor equal to the number of mesh points of the quadrupole subspace $\{\alpha_{20}, \alpha_{22}\}$ for a fixed octupole configuration. Now we come to the definition of the collective Hamiltonian in question. A realistic and quantized quadrupole-octupole-vibrational collective Hamiltonian with varying mass parameters and moments of inertia can be defined as

$$
\mathcal{H}_{\text{coll}}(\alpha_2, \alpha_3, \Omega) = \frac{-\hbar^2}{2} \Bigg\{ \frac{1}{\sqrt{|B_2|}} \sum_{\nu\nu'=0}^{2} \frac{\partial}{\partial \alpha_{2\nu}} \sqrt{|B_2|} \big[B_2^{-1} \big]^{\nu\nu'} \frac{\partial}{\partial \alpha_{2\nu'}}
$$
$$
+ \frac{1}{\sqrt{|B_3|}} \sum_{\mu\mu'=0}^{3} \frac{\partial}{\partial \alpha_{3\mu}} \sqrt{|B_3|} \big[B_3^{-1} \big]^{\mu\mu'} \frac{\partial}{\partial \alpha_{3\mu'}} \Bigg\}
$$
$$
+ \hat{H}_{\text{rot}}(\Omega) + \hat{V}(\alpha_2, \alpha_3), \qquad (18)
$$

where α_2 and α_3 describe symbolically the subspaces of the quadrupole and octupole collective variables with metrics; $B_2(\alpha_2)$, $B_3(\alpha_3)$ denote the quadrupole and octupole microscopic mass tensor, respectively; and $|B_2| = \det B_2(\alpha_2)$, $|B_3| = \det B_3(\alpha_3)$. Those microscopic symmetric mass tensors are determined using a commonly used *cranking* approximation [36], which has been widely used in the nuclear structure physics. Its covariant $(\lambda\nu, \lambda\nu')$ component for $\lambda = 2$ or $\lambda = 3$ and indices $\mu > 0$ is given by the formula

$$
B_{\lambda\nu, \lambda\nu'}(\{\alpha_{\lambda\mu}\})
$$
$$
= \sum_{kl} \frac{\langle \phi_k | \frac{\partial \hat{H}_{sp}}{\partial \alpha_{\lambda\nu}} | \phi_l \rangle \langle \phi_l | \frac{\partial \hat{H}_{sp}}{\partial \alpha_{\lambda\nu'}} | \phi_k \rangle}{(E_k + E_l)^3} (u_k v_l + v_k u_l)^2, \quad (19)
$$

where the double sum runs over the full set of BCS (Bardeen–Cooper–Schrieffer) quasiparticle (qp) (including time-reversed) states obtained from the eigensolutions of the chosen mean-field Hamiltonian $\hat{H}_{sp}$ and using a pairing approach. Quantities v_n are the occupation probability amplitude of the nth qp state while u_n is obtained through the relation $u_n^2 = 1 - v_n^2$. Quantities E_k and E_l in the denominator of Eq. (19) are the quasiparticle energies of kth and lth states.

Nowadays, the potential energy of a nucleus in collective variable space is usually obtained within various elaborate self-consistent microscopic approaches. In this work, an effective approximation to generate the collective potential in the six-dimensional space of $\{\alpha_2, \alpha_3\}$ variables is still a widely applied macroscopic-microscopic model. This model, for a reasonable choice of predefined mean-field potential, pairing interaction and the smooth liquid-drop energy formula, is able to produce reliable estimates of potential energy surfaces $\hat{V}(\alpha_{2\nu}, \alpha_{3\mu})$. Within these studies we use the Woods-Saxon potential [37] with the so-called *universal* set of parameters [19] (refitted to the newer single particle data in Ref. [38])

which delivers the single-particle energies and eigenstates for a given mean-field deformation. Both those quantities are the starting point to the calculations of quantum shell and pairing energies and mass parameters via Eq. (19).

The shell-energy correction arising due to the shell structure of single nucleons is calculated using the traditional Strutinsky approach of sixth order [39–41]. In turn, for the pairing energy, the particle number projected BCS approach [42,43] is applied. Finally, the leading liquid-drop energy term is developed here by the Lublin-Strasbourg Drop formula (LSD) [44] which permits us to successfully reproduce fission barriers of actinide nuclei, see, e.g., Ref. [45]. For more details of the macroscopic-microscopic model used here, please refer to Sec. V A.

V. ROTATIONAL HAMILTONIAN

As we have already mentioned, due to significantly differing energy scales of the vibrational and rotational modes, they are assumed here to be entirely decoupled. As a result, the rotational term $\hat{H}_{\text{rot}}(\Omega)$ depends only on the Euler angles and the static shape of the nucleus, here corresponding to the ground state. Since, as discussed in Sec. III B, also the rotational Hamiltonian term has to be scalar with respect to the symmetrization group $\bar{G}_s$, it is convenient to construct it out of the irreducible tensors of the $\bar{G}_s$ symmetry group as done, e.g., in Refs. [31,46]. Such tensors with respect to the SO(3) group can be built from the angular-momentum tensor components defined in the body-fixed frame $\hat{J}_{\pm 1} = \mp \frac{1}{\sqrt{2}} (\hat{J}_x \mp i \hat{J}_y)$, $\hat{J}_0 = \hat{J}_z$ in the following way:

$$
\hat{T}_{\lambda\mu}(n; \lambda_2 = 2, \lambda_3 = 3, \ldots, \lambda_{n-1} = (n-1))
$$
$$
\equiv \big[(((\hat{J} \otimes \hat{J})_{\lambda_2} \otimes \hat{J})_{\lambda_3} \otimes \ldots \otimes \hat{J})_{\lambda_{n-1}} \big]_{\lambda\mu}, \quad (20)
$$

where n is the rank of the resulting tensor, λ_k for $k = 2, 3, \ldots, n - 1$ are the multipolarities of the tensors arising within the intermediate couplings, while λ is the multipolarity of the resulting tensor. The coupling of tensors of multipolarity $\lambda = 1$ in Eq. (20) is obtained within the standard expression containing the SO(3) Clebsch-Gordan coefficients $(1, \mu; 1, \mu' | \lambda_2 \mu_2)$

$$
(\hat{J} \otimes \hat{J})_{\lambda\mu} = \sum_{\mu=-1}^{1} \sum_{\mu'=-1}^{1} (1\mu 1\mu' | \lambda\mu) \hat{J}_{1\mu} \hat{J}_{1\mu'}. \quad (21)
$$

The way of constructing the irreducible tensors (20) is not unique due to the fact that the set of intermediate tensors $\{\lambda_2, \lambda_3, \ldots\}$ can be chosen arbitrarily, remembering only that the "triangle rule" $\lambda_k - 1 \leqslant \lambda_{k+1} \leqslant \lambda_k + 1$, for $k = 1, 2, \ldots n$, has to be satisfied.

It turns out, however, that for the construction of the physically relevant *generalized* rotor Hamiltonians, only the tensors for which $n = \lambda$ are important. The exception is single term $T_{00} (n = 2)$, which is indispensable to reproduce the crude energies of the rotational spectrum.

In this context, the word "generalized" means that we go beyond with the properties of the standard $\bar{D}_2$-symmetric triaxial rotors.

The rotor Hamiltonian $\hat{\mathcal{H}}_{\mathrm{rot}}$ of given symmetry $\bar{G}$ and multipolarity λ can be therefore constructed with the help of the irreducible tensor operators with $n = \lambda$ as their linear combination over λ and μ indices and the term $T_{00}(n = 2)$ as

$$\hat{\mathcal{H}}_{\mathrm{rot}} = \sum_{\lambda=0}^{\lambda_{\max}} \sum_{\mu=-\lambda}^{\lambda} c_{\lambda\mu} \hat{T}_{\lambda\mu} + c_{00} T_{00}(n = 2). \quad (22)$$

The upper limit of multipolarities $\lambda_{\max}$ is, in principle, arbitrary. Requiring the invariance of the $\hat{\mathcal{H}}_{\mathrm{rot}}$ in Eq. (22) with respect to a given symmetry $\bar{G}$ and $\bar{g} \in \bar{G}$, the coupling constants $c_{\lambda\mu}$ have to fulfill the following system of equations:

$$\sum_{\mu} c_{\lambda\mu} \left[\delta_{\mu\nu} - D_{\nu\mu}^{\lambda*}(g) \right] = 0, \quad \nu = \{-\lambda, \ldots, +\lambda\}, \quad (23)$$

where $D_{\nu\mu}^{\lambda*}(g)$ denotes the complex conjugated Wigner function of group element g. Quantities $c_{\lambda\mu}$ are generally complex numbers, except for C_{00}, which is always real and depends on the scalars of the $\overline{SO}(3)$ group, i.e., the square of the angular-momentum value I^2.

The hermiticity condition $\hat{\mathcal{H}}_{\mathrm{rot}} = \hat{\mathcal{H}}_{\mathrm{rot}}^{\dagger}$ applied to (22) leads to the condition

$$c_{\lambda-\mu} = (-1)^{\mu} c_{\lambda\mu}^{*}, \quad (24)$$

reducing the number of independent coefficients $c_{\lambda\mu}$. In the case of the traditional quadratic, triaxial rotor Hamiltonian of dihedral symmetry D_2, the coupling constants c_{00}, c_{20}, and c_{22} are independent and defined by the moments of inertia as

$$c_{00} = -\frac{1}{\sqrt{12}} \left(\frac{1}{I_x} + \frac{1}{I_y} + \frac{1}{I_z} \right),$$

$$c_{20} = \frac{1}{\sqrt{6}} \left(\frac{1}{I_z} - \frac{1}{2I_x} - \frac{1}{2I_y} \right), \quad (25)$$

$$c_{22} = \frac{1}{4} \left(\frac{1}{I_x} - \frac{1}{I_y} \right),$$

where I_x, I_y, I_z are the microscopic nuclear moments of inertia with respect to the OX, OY, and OZ axes, respectively. These moments, similarly to the mass parameters in Eq. (19), are obtained within the cranking approximation [36] using the Woods-Saxon mean-field and the projected BCS model, as discussed in Sec. IV.

If the $\bar{D}_4$-symmetric rotor Hamiltonian is needed, as $\hat{H}_{\mathrm{rot}}(\Omega)$ in Eq. (18), then one should solve Eq. (23) to determine the coupling constants $c_{\lambda\mu}$ entering Eq. (22). Solving Eq. (23) for the lowest value of multipolarity $\lambda = 2$, we get the relation between c_{20} and c_{22} which may be estimated by formula

$$c_{22} \approx c_{20}/0.8165, \quad (26)$$

valid for an arbitrary c_{20}. Its value has been adjusted to ensure the energy distance of the lowest rotational states in the ground-state band to be comparable with their experimental values in the ^{156}Gd nucleus.

Let us calculate the matrix elements of the Hamiltonian (22) in the orthonormal basis of complex conjugated Wigner

functions

$$f_{MK}^{J}(\Omega) = \sqrt{2J+1} \sum_{K=-J}^{J} D_{MK}^{J*}(\Omega). \quad (27)$$

The reduced matrix elements of the tensors $\hat{T}_{\lambda\mu}$ are expressed as

$$\langle J || \hat{T}_{\lambda}(n; \{\lambda\}_n) || J \rangle$$
$$= F(J, \lambda_{n-1}, \lambda_n) \langle J || \hat{T}_{\lambda_{n-1}}(n-1; \{\lambda\}_{n-1}) || J \rangle \langle J || \hat{I} || J \rangle, \quad (28)$$

and transformed into normal matrix element by means of the Wigner-Eckart theorem to the form

$$\langle J'M' | \hat{T}_{\lambda\mu}(n; \{\lambda\}_n) | JM \rangle = \langle J' || \hat{T}_{\lambda}(n; \{\lambda\}_n) || J \rangle$$
$$\times (JM\lambda\mu | J'M') / \sqrt{2J'+1}.$$

The scalar function F in Eq. (28), for arbitrary values of K, K', and μ, is given as

$$F(J, \lambda_{n-1}, \lambda_n) = \sqrt{2J+1} \, (JJ\lambda 0 | JJ))^{-1}$$
$$\times \sum_{\mu'=0}^{1} (\lambda_{n-1}\mu' 1 - \mu' | \lambda 0)(JJ - \mu'\lambda_{n-1}\mu' | JJ)$$
$$\times (JJ1 - \mu' | JJ - \mu'). \quad (29)$$

As an example, let us write down explicitly the reduced matrix elements of the tensors $\hat{T}_{\lambda\mu}(n; \{\lambda\}_n)$ of the lowest ranks:

$$n = 1, \quad \langle J || \hat{J} || J \rangle = \sqrt{J(J+1)(2J+1)}$$
$$n = 2, \quad \langle J || \hat{T}_{\lambda}(2) || J \rangle = F(J, 1, \lambda) \langle J || \hat{J} || J \rangle^2$$
$$n = 3, \quad \langle J || \hat{T}_{\lambda}(3, \lambda_2) || J \rangle = F(J, 1, \lambda_2) F(J, \lambda_2, \lambda)$$
$$\times \langle J || \hat{J} || J \rangle^3. \quad (30)$$

As we deduce from Eq. (31), the matrix elements of Eq. (28) are defined in a recursive way.

A. Construction of the collective basis

In the previous section, we apply the adiabatic approximation which leads to separation of the vibrational and rotational motions. Following this idea, the basis in which the Hamiltonian (18) is diagonalized contains the symmetrized with respect to intrinsic $\bar{D}_4$ group harmonic-oscillator eigensolutions coupled with an appropriate Wigner function. The latter carries out the spin dependence of the full vibrational-rotational basis state. Let us note that only real parts of complex $\alpha_{3\mu}$ collective variables are considered in this work. The kth, $k = 1, 2, \ldots$, initial (before symmetrization) function used to generate the orthogonal vibrational-rotational basis state, depending on spin J and its projections M and K, is chosen as

$$\Psi_{k;JMK}^{(\pm)}(\alpha_2, \alpha_3, \Omega)$$
$$= u_{n_{20}}(\eta_{20}, \alpha_{20} - \alpha_{20}^{\circ}) u_{n_{22}}(\sqrt{2}\eta_{22}, \alpha_{22}$$
$$- \alpha_{22}^{\circ}) u_{n_{30}}(\eta_{30}, \pm\alpha_{30} - \alpha_{30}^{\circ}) u_{n_{31}}(\sqrt{2}\eta_{31}, \pm\alpha_{31} - \alpha_{31}^{\circ})$$
$$\times u_{n_{32}}(\sqrt{2}\eta_{32}, \pm\alpha_{32} - \alpha_{32}^{\circ}) u_{n_{33}}(\sqrt{2}\eta_{33},$$
$$\pm\alpha_{33} - \alpha_{33}^{\circ}) R_{MK}^{J}(\Omega), \quad (31)$$

with $R_{MK}^J(\Omega)$ given by (27) and u_m denoting the m-phonon normalized one-dimensional oscillator eigensolution of shifted collective argument $\alpha_{\lambda\mu} - \overset{\circ}{\alpha}_{\lambda\mu}$,

$$u_m(\eta, \overset{\circ}{\alpha}; \alpha) = \sqrt{\frac{\eta}{2^m \sqrt{\pi}\, m!}}\, H_m(\eta\alpha)\, e^{-\frac{1}{2}\eta^2(\alpha - \overset{\circ}{\alpha})^2}. \quad (32)$$

The function $H_m(\eta\alpha)$ denotes the standard Hermite polynomial of mth order, whereas η is the so-called "width" parameter. Note that, as in Sec. IV, α_2, α_3 denote the full sets of quadrupole and octupole variables of the model, respectively. The $\sqrt{2}$ factor in front of $\eta_{\lambda\nu}$ for $\nu > 0$ in Eq. (31) introduces the "scaling" of the corresponding variable according to the metrics $g^{(\lambda)}$.

In the current investigations, depending on the parity of the basis state, we admit the phonon number of the quadrupole and octupole functions u_m, which for the ground-state band are

$$\sum_{\kappa=0}^{3} n_{3\kappa} = 0, \quad \kappa = \{0, 1, 2, 3\},$$
$$n_{20} + n_{22} = \{0, 1, \dots, 6\}, \quad (33)$$

while, for the negative-parity octupole band, they are

$$\sum_{\kappa=0}^{3} n_{3\kappa} = \{1, 3\}, \quad \kappa = \{0, 1, 2, 3\},$$
$$n_{20} + n_{22} = 0. \quad (34)$$

The free basis parameters are therefore $\eta_{20}, \eta_{22}, \eta_{3\rho}$ and the corresponding argument shifts $\overset{\circ}{\alpha}_{20}, \overset{\circ}{\alpha}_{22}, \overset{\circ}{\alpha}_{3\rho}$ for $\rho = \{0, 1, 2, 3\}$.

Applying the projection onto the given parity operator

$$\mathcal{P}^{\pm} = \tfrac{1}{2}(\hat{I} \pm \hat{C}_i) \quad (35)$$

with $\hat{C}_i$ and $\hat{I}$ denoting, respectively, the inversion and the identity operations, the basis functions of positive or negative parity are given as the following combinations of functions (31):

$$\Psi_{k;JMK\pi=\pm 1}(\alpha_2, \alpha_3, \Omega)$$
$$= \tfrac{1}{2}[\Psi_{k;JMK}^{(+)}(\alpha_2, \alpha_3, \Omega) \pm \Psi_{k;JMK}^{(-)}(\alpha_2, \alpha_3, \Omega)], \quad (36)$$

where numbers $\pi = +1$ and $\pi = -1$ correspond, respectively, to the even- and odd-parity functions.

Now, we can switch on the symmetrization of the basis state using the projection onto the demanded irreducible representation Γ of a given symmetry group method. Such a projection onto the representation Γ of the symmetrization intrinsic group $\bar{G}_s$ is performed with the help of the Hermitian projection operator defined as in Ref. [26],

$$\hat{P}^{\Gamma} = \frac{\dim(\Gamma)}{\mathrm{card(G)}} \sum_{\bar{g} \in \bar{G}_s} \chi^{\Gamma}(\bar{g})^{\star} \hat{\bar{g}}, \quad (37)$$

where $\bar{g}$ belongs to the group $\bar{G}_s$ containing $\mathrm{card}(\bar{G}_s)$ elements. The quantity $\chi^{\Gamma}(\bar{g})$ is the character of the element $\bar{g}$ in the irreducible representation Γ. The $\dim(\Gamma)$ is the dimension of this representation, which, for the scalar representation $\Gamma = A1$, is $\dim(A1) = 1$. The formula (37) is valid in both the laboratory and the intrinsic reference frames under the

condition that the matrices corresponding to the elements $\bar{g}$ of the intrinsic group are transposed with respect to the laboratory group elements.

In numerical calculations, it is very useful that the projection operator is idempotent, i.e., $(\hat{P}^{\Gamma})^2 = \hat{P}^{\Gamma}$. This property, together with the commutation relation $[\hat{P}^{\Gamma}, \hat{O}] = 0$, where the operator $\hat{O}$ describes a demanded observable, allows us to calculate the matrix elements between projected states $\langle \Psi_k | \hat{P}^{\Gamma} \hat{O} \hat{P}^{\Gamma} | \Psi_{k'} \rangle$ as equal to the element between a projected and unprojected functions, $\langle \Psi_k | \hat{O} \hat{P}^{\Gamma} | \Psi_{k'} \rangle = \langle \Psi_k | \hat{P}^{\Gamma} \hat{O} | \Psi_{k'} \rangle$.

The actions of the operator $\hat{\bar{g}}$ onto an arbitrary functions of α and Ω variables are defined for intrinsic groups in Eq. (9).

Applying operator (37), projecting the function (36) onto the scalar (denoted by A1) representation of our symmetrization group $\bar{D}_4$, one gets

$$\Psi_{k;JM\kappa\pi}^{(A1)} = \hat{P}^{(A1)} \Psi_{k;JMK\pi} = \sqrt{2J+1} \sum_{i=1}^{\mathrm{card}(\bar{D}_4)} \frac{\dim(A1)}{\mathrm{card}(\bar{D}_4)}$$

$$\times \sum_{K=-J}^{J} D_{\kappa K}^J(\bar{g}_i) D_{MK}^{J*}(\Omega) u_{n_{20}}(\eta_{20}, \hat{\bar{g}}_i \alpha_{20} - \overset{\circ}{\alpha}_{20})$$

$$\times u_{n_{22}}(\sqrt{2}\eta_{22}, \hat{\bar{g}}_i \alpha_{22} - \overset{\circ}{\alpha}_{22}) u_{n_{30}}(\eta_{30}, \hat{\bar{g}}_i \alpha_{30} - \overset{\circ}{\alpha}_{30})$$

$$\times u_{n_{31}}(\sqrt{2}\eta_{31}, \hat{\bar{g}}_i \alpha_{31} - \overset{\circ}{\alpha}_{31}) u_{n_{32}}(\sqrt{2}\eta_{32}, \hat{\bar{g}}_i \alpha_{32} - \overset{\circ}{\alpha}_{32})$$

$$\times u_{n_{33}}(\sqrt{2}\eta_{33}, \hat{\bar{g}}_i \alpha_{33} - \overset{\circ}{\alpha}_{33}), \quad (38)$$

where the action of the element $\hat{\bar{g}}$ onto the rotational function $R_{MK}^J(\Omega)$ is given by Eq. (9). Finally, since $\hat{\bar{g}}_i$ operators do not couple the quadrupole, octupole, and rotational spaces, we can rewrite the projected function (38) to an abbreviated form,

$$\Psi_{k;JM\kappa\pi}^{(A1)} \equiv \phi_{n\pi}(\alpha_2, \alpha_3)\, \tilde{R}_{M\kappa}^J(\Omega). \quad (39)$$

Note that the right-hand side of Eq. (9) is summed over all possible projections of angular-momentum number K. As a result, for function (38), K is not a good quantum number. If we admit, for fixed parity π, that in the body-fixed frame the M number may be chosen arbitrarily within the range $-J \geqslant M \leqslant J$, then the only number that allows us to identify the basis states (38) is κ, changing also within the range $-J \geqslant \kappa \leqslant J$. For the practical calculations, it is important that the operator (37) does not change the parity π of the initial state (31) since any rotation operation $\bar{g}$ entering Eq. (37) commutes with the parity operator of Eq. (35).

B. Orthogonalization of projected states

The projection operator (37) presented in Sec. V A, applied onto different functions defined through Eq. (36), does not assure the orthogonality of the resulting functions, say, $\Psi_k^{(A1)}$, i.e.,

$$\langle \Psi_k^{(A1)} | \Psi_{k'}^{(A1)} \rangle \neq \delta_{kk'}, \quad (40)$$

although all initial $\{\Psi_k\}$'s are chosen here to be orthonormal.

An efficient orthogonalization could be done by standard Gram-Schmidt procedure described, e.g., in Ref. [47] or by diagonalization of the so-called Gramm matrix, applied, e.g., in the generator coordinate method, described in Ref. [48]. In our opinion, the latter turns out to be more efficient since

it immediately allows us to identify the linearly dependent functions in the function set. Such functions should, certainly, be removed from the basis. Now, let us schematically describe this method.

Generally, in the N_Q-dimensional Hilbert space of nonorthogonal states $\{Q\}$, one can introduce the positive defined overlap operator $\hat{\mathcal{N}}$ of the form [48]

$$\hat{\mathcal{N}} = \sum_{q \in \{Q\}} |q\rangle\langle q|, \tag{41}$$

where, obviously, its expectation value for an arbitrary state $|\phi\rangle \in \{Q\}$ is equal to

$$\langle \phi|\hat{\mathcal{N}}|\phi\rangle = \sum_{\{Q\}} \langle \phi|q\rangle\langle q|\phi\rangle = \sum_{\{Q\}} |\langle q|\phi\rangle|^2 \geqslant 0. \tag{42}$$

The eigenproblem of the $\hat{\mathcal{N}}$ operator is therefore given in the form

$$\sum_q |q\rangle\langle q|w_l\rangle = \lambda_l|w_l\rangle, \tag{43}$$

where $\{|w_n\rangle\}$ and $\{\lambda_n\}, n = 1, 2 \cdots N_Q$ correspond, respectively, to the eigenvectors and eigenvalues of the $N_Q \times N_Q$ Gramm matrix. Now, to transform the above equation to the matrix form, we multiply both sides of Eq. (43) by a *bra* vector $\langle q'|$,

$$\sum_q \langle q'|q\rangle\langle q|w_l\rangle = \lambda_l\langle q'|w_l\rangle, \tag{44}$$

where $\langle q'|q\rangle$ is the overlap matrix and $\tilde{w}_{lq'} \equiv \langle q'|w_l\rangle$ is the column corresponding to the N_Q-dimensional lth eigenvector.

The orthonormal space of vectors $|b_k\rangle, k = 1, 2, \ldots, N_Q$ constructed with the help of states q is given as

$$|b_l\rangle = \frac{1}{\sqrt{\lambda_l}} \sum_{q'} \tilde{w}_{lq'}|q'\rangle. \tag{45}$$

The above general formalism can be directly applied to our functions given by Eq. (38) to obtain the orthonormalized, $A1$-symmetric collective basis, used later to diagonalize the collective Hamiltonian (18).

In our numerical calculations, it happens that some of the eigenvalues λ_n of Eq. (44) are equal to zero (strictly speaking, they are several orders of magnitude smaller than the others). This indicates that in the set $\{Q\}$ there exist unwanted linearly dependent subspaces. In our model, for given spin J, parity π, and the phonon number imposed by conditions (33) and (34), the pairs of states (38) with κ and $-\kappa$ numbers are identified to be linearly dependent. The final basis, certainly, should contain only one such state, either with κ or $-\kappa$.

VI. CENTER-OF-MASS MOTION AND ELECTRIC TRANSITION OPERATORS

The octupole deformation of the nucleus induces the change of the center-of-mass position as function of deformation. This implies that, besides the collective quadrupole and octupole vibrations and rotations treated in the proposed model, our nucleus as a whole performs a kind of periodic translational

motion. The kinetic energy of such a mode is not explicitly included in the collective Hamiltonian (18).

However, we investigate on average the effect of the center-of-mass motion on the $B(E1)$ and $B(E2)$ probabilities, which are the quantities of our interest, by including the dipole (with $\lambda = 1$) degrees of freedom, $\alpha_{1\rho}$, $\rho = \{-1, 0, +1\}$ into the dipole and quadrupole transition operators defined in Sec. VIII. Those parameters are believed to be mainly responsible for the center-of-mass motion. Nonetheless, as shown [49], their large-enough values are also able to significantly modify the shape of nuclear drop, affecting also the total nuclear potential energy surface.

The center-of-mass (c.m.) vector $\vec{r}_{\text{c.m.}} = \vec{r}_{\text{c.m.}}(\alpha_{1\mu}, \alpha_{20}, \alpha_{22}, \{\alpha_{3\nu}\})$ of a nucleus of total mass M and nuclear density $\rho(\vec{r})$, defined in a standard way as

$$\vec{r}_{\text{c.m.}} = \frac{1}{M} \int_V \vec{r}\rho(\vec{r})d^3\vec{r}, \tag{46}$$

are, as easily deduced from Eq. (46), the four order polynomials in $\alpha_{1\mu}$ with the coefficients dependent on the other remaining, quadrupole and octupole, parameters. These polynomials are solved with respect to the variables $\alpha_{1\mu}$ with the condition $\vec{r}_{\text{c.m.}} = 0$,

$$\alpha_{1\mu} = \alpha_{1\mu}(\vec{r}_{\text{c.m.}} = 0, \alpha_{20}, \alpha_{22}, \{\alpha_{3\nu}\}). \tag{47}$$

Calculated in this way $\alpha_{1\mu}$'s as a function of $\alpha_{2\nu}$ and $\alpha_{3\nu'}$, inserted into Eq. (4), ensure that the nuclear surface is defined in the center-of-mass frame. The above consideration indicates also that the above-mentioned quadrupole and octupole deformations are still the only independent collective variables of our model.

The influence of dipole deformation parameters on the properties of atomic nuclei are discussed relatively rarely in the literature. As an example, the authors of recent work (in Ref. [49]) discussed the influence of $\alpha_{1\nu}$ on the potential energy surface of Thorium isotopes.

Figure 1 shows the evolution of the nuclear shape [cuts by (OX, OZ) plane of OZ axially symmetric nucleus] as a function of the α_{10} parameter for the fixed other deformations: $\alpha_{20} = 0.25$ (top) and $\alpha_{20} = 0.8$ (bottom) and, in both cases, $\alpha_{30} = 0.3$ and $\alpha_{3\nu} = 0$, $\nu = \{1, 2, 3\}$.

The increase of α_{10} values leads to more and more compact shapes and, by consequence, lower energy. In the extreme, this process may bring the nucleus to the spherical form. In contrast, in Fig. 2 we have shown the change of the nuclear shape obtained with $\alpha_{3\nu} = 0$, $\nu = \{1, 2, 3\}$, $\alpha_{10} = 0$, $\alpha_{20} = 0.8$, and $\alpha_{30} = 0.3$ plotted for several values of the α_{11} parameter. This nonaxial deformation is seen to be responsible for creating neck-in shapes. Such a feature can be interesting since, even very compact shapes with significantly large values of α_{11} can split into two parts; see the curve for $\alpha_{11} = 1.0$.

Let us show the numerical solutions of Eq. (47) on the six-dimensional mesh of $\{\alpha_{20}, \alpha_{22}, \alpha_{3\mu}\}$ deformations. First, for each point of the six-dimensional mesh, the center-of-mass shift $\vec{r}_{\text{c.m.}}$ is calculated and then the dipole parameters α_{10} and α_{11} that mimic this shift are found.

The dipole α_{10} and α_{11} variables induced by couplings of, in general, considered all six degrees of freedom are shown
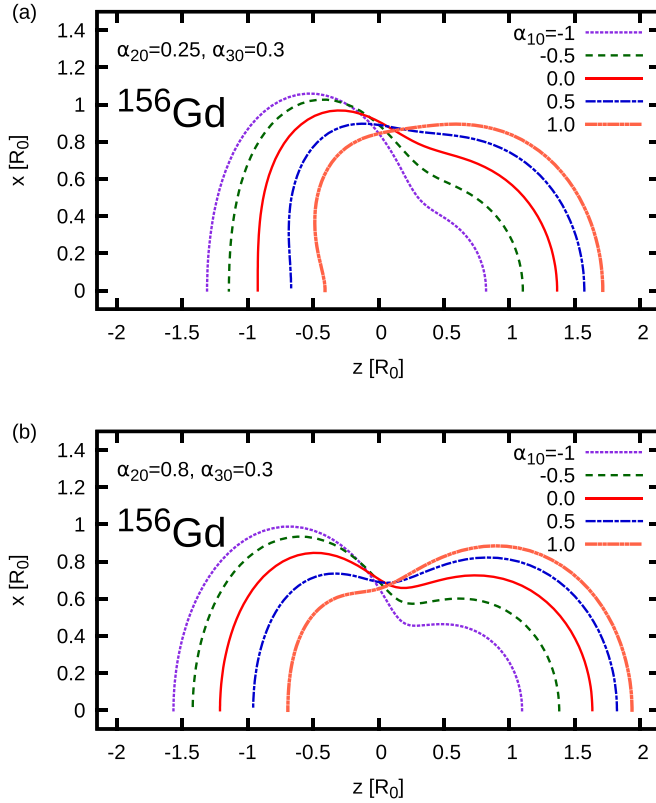
FIG. 1. Influence of α_{10} deformation parameter on the shapes of the nucleus [here (OX, OZ) cuts are shown] in two cases: (a) for $\alpha_{20} = 0.25$ corresponding to the ground-state minimum of ^{156}Gd and (b) for $\alpha_{20} = 0.8$. In both cases, the only nonzero octupole deformation is $\alpha_{30} = 0.3$.

in Fig. 3. However, more detailed studies reveals that α_{10} is induced only by the axial octupole α_{30} parameter for other five octupole and quadrupole parameters equal to zero. Similarly, α_{11} arises solely due to the presence of the α_{31} one.

To sum up, in Fig. 3 we can observe the direct dependence of induced dipole deformations α_{10} and α_{11} on axial α_{30} and nonaxial α_{31} octupole degrees of freedom alone, respectively, whereas Fig. 4 presents the influence of combinations of the axial α_{20} and α_{30} parameters on induced α_{10}.
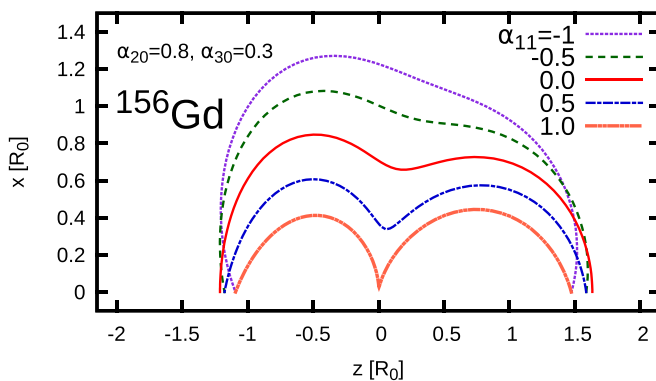

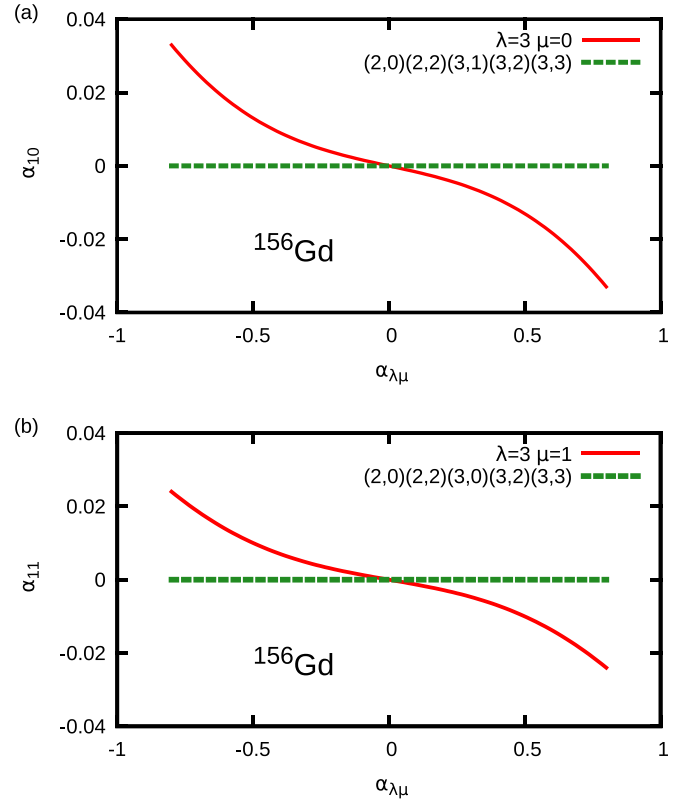FIG. 2. Same as in Fig. 1 but α_{11} values are changed.

FIG. 3. Dependence of the dipole axial α_{10} (a) and nonaxial α_{11} (b) on the octupole deformation parameters α_{30} and α_{31} with other quadrupole and octupole deformations set to zero.

Comparing Figs. 3 and 4 we can learn that for quadrupole deformations equal to zero, the values of α_{10} as a function of α_{30} varies within the range of $(-0.04, +0.04)$ while, for extremely elongated nucleus with $\alpha_{20} = \approx \pm 1.0$, $\alpha_{10} \in (-0.5, +0.5)$. Briefly, the larger nuclear elongation, the stronger the dipole deformation that is induced.
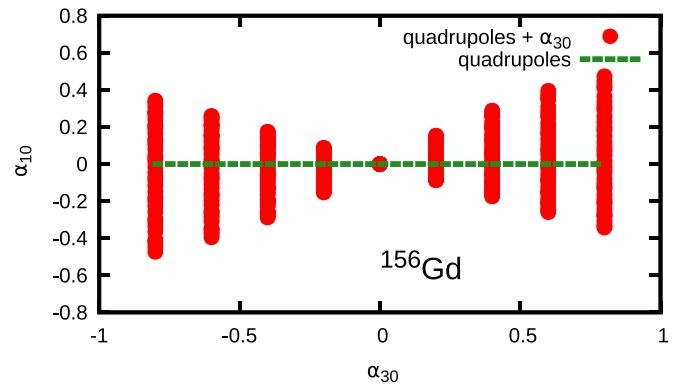

FIG. 4. Values of the induced α_{10} parameter obtained from the center-of-mass shift for different combinations of α_{20} and α_{30} parameters by the other deformations set to zero. Each vertical thick (red) line corresponds to fixed α_{20} changing from $\alpha_{20} = -1.0$ (extreme left line) to $\alpha_{20} = +1.0$ (extreme right line) by the step of 0.25.

VII. COLLECTIVE POTENTIAL

Over the years, considerable effort has been made to calculate the potential energy of a nucleus as a function of its geometrical shape. It is clear that the most adequate approach to calculate this energy would be to start with a carefully chosen effective nucleon-nucleon interaction and solve the resulting many-body problem. Although there has been great progress in computational techniques recently, the constrained self-consistent calculation with more than three independent constraints, imposed, e.g., on multipole moments of mass-distribution density, is still a challenging task.

A. Macroscopic-microscopic method

In this work the estimates of the total energy of the deformed nucleus are therefore done within the phenomenological nuclear mean-field approach, known as the so-called macroscopic-microscopic method of Strutinsky. Note that in this method the total nuclear potential energy is composed of the macroscopic energy term given usually by the liquid-drop-type energy and the microscopic, shell, and pairing energy corrections describing quantum effects in a nucleus. Despite the fact that this kind of approach has been applied since the early 1960s, it is still a powerful and successful tool, well suited particularly to large-scale calculations and able to produce results close to the experimental data. The details of these kinds of calculations and corresponding results are presented, e.g., in Refs. [50–54].

One usually applies an adequate type of liquid drop model and the mean-field potential to reproduce the results possibly in the best way. Nevertheless, the topology of the potential energy surfaces obtained in the vicinity of the equilibrium state of cold medium mass nuclei generated, for example, by the finite range droplet model (FRLDM) [55,56] or the Lublin-Strasbourg model (LSD) [44], is very similar.

The FRLDM model looks to be slightly more involved (thus a little more time-consuming) than the LSD one, and the collective potential calculations on six-dimensional deformation mesh of about 2×10^6 points have been performed with the use of the LSD approximation.

In turn, the microscopic energy of the nucleus is defined as the sum of the shell and pairing energy corrections to the liquid drop smoothly changing energy. The shell energy is obtained from the Strutinsky method developed in Refs. [39–41]. For the pairing energy [42,43] as the difference between the sum of the single-particle energies and the energy of the pair correlations [55], the particle-number projected pairing model [43] within the standard BCS framework is applied.

The BCS wave function has the form:

$$|\mathrm{BCS}\rangle = \prod_m (u_m + v_m \hat{a}_m^+ \hat{a}_{\bar{m}}^+)|0\rangle, \tag{48}$$

where the $|0\rangle$ is the particle vacuum, $v_m(u_m)$ are the occupation (nonoccupation) numbers of the state m and $\hat{a}_m^+, \hat{a}_{\bar{m}}^+$ are the creation operators of the quassiparticles on top of mth single-particle state and its time-reversed counterpart, respectively. Index m runs over the states belonging to the so-called *pairing window*.

The particle-number-projected (PBCS) wave function can be written with the use of appropriate projection operator as

$$|\mathrm{PBCS}\rangle = \frac{1}{2\pi} \int_0^{2\pi} e^{-i\phi N} \prod_n (u_n + e^{2i\phi} v_n \hat{a}_n^+ \hat{a}_{\bar{n}}^+)|0\rangle, \tag{49}$$

where N is the number of particles in the system and ϕ is the rotation angle in the so-called *gauge space*. Function (49) is used to obtain the energy of the nucleus as the expectation value of the BCS Hamiltonian

$$E_{\mathrm{PBCS}} = \frac{\langle \mathrm{PBCS}|\hat{H}|\mathrm{PBCS}\rangle}{\langle \mathrm{PBCS}|\mathrm{PBCS}\rangle}, \tag{50}$$

where $\hat{H}$ is the many-body BCS Hamiltonian. As a result of evaluating Eq. (50), we may come to the expression for the total nuclear energy E_{PBCS} arising from the pairing interaction in the nucleus

$$E_{\mathrm{PBCS}} = \sum_{\nu=\mathcal{N}_1}^{\mathcal{N}_2} 2 v_\nu^2 (e_\nu - \lambda) - \frac{\Delta^2}{G} - \sum_{\nu=\mathcal{N}_1}^{\mathcal{N}_2} (e_\nu - \lambda)$$
$$- G \left(\sum_{\nu=\mathcal{N}_1}^{\mathcal{N}_2} v_k^4 - \sum_{\nu=\mathcal{N}_1}^{\mathcal{N}_2} 1 \right), \tag{51}$$

and the so-called average pairing correction

$$\overline{E}_{\mathrm{pc}} = -\frac{1}{4} \frac{N^2}{\overline{\rho}} \left\{ \sqrt{1 + \frac{2\overline{\rho}\overline{\Delta}}{N}} - 1 \right\}$$
$$+ \frac{1}{2} \overline{\rho}\, \overline{\Delta}\, \overline{G} \arctan \frac{N}{2\overline{\rho}\overline{\Delta}}, \tag{52}$$

where $\mathcal{N}_1$ and $\mathcal{N}_2$ are the lower and upper limits of the pairing window, v_ν^2 is the occupation probability of νth quasiparticle state, $\overline{\rho}$ is the mean density distribution of single-particle states, and G is the strength of the pairing interaction [57]. The average proton and neutron energy gaps, $\overline{\Delta}_p$ and $\overline{\Delta}_n$, are fitted to the experimental separation energy differences [58] and are given as

$$\overline{\Delta}_n = 9.08/\sqrt{A} \text{ MeV}, \quad \overline{\Delta}_p = 9.85/\sqrt{A} \text{ MeV}. \tag{53}$$

Finally, the full pairing correction energy in the projected BCS model is defined as

$$E_{\mathrm{pair}} = E_{\mathrm{BCS}} + \overline{E}_{\mathrm{pc}}. \tag{54}$$

In order to calculate the pairing energy correction $\Delta E_{\mathrm{BCS}}^{(q)}$ ($q = n$ for neutrons and $q = p$ for protons) as a component of the macroscopic-microscopic approach, we subtract the energy $E_{\mathrm{pair}}^{(q)}$ given by Eq. (54) from the sum of single-particle levels and its time-reversed partners separately for protons and neutrons,

$$\Delta E_{\mathrm{BCS}}^{(q)} = \sum_{\mu=1}^{N_F^{(q)}} e_\mu^{(q)} - E_{\mathrm{pair}}^{(q)}, \tag{55}$$

with $N_F^{(q)}$ denoting the Fermi level of the proton or neutron distribution. Clearly, the total energy correction is the sum of both the proton and neutron contributions.

The single-particle energies e_ν used to calculate the shell and pairing energies are the solutions of the Schrödinger equation with the mean-field Hamiltonian of the Woods-Saxon form [37]. The latter is developed with the use of the so-called *universal* set of parameters [19], refitted to the newest experimental data and presented in Ref. [38].

Having defined all the components of the macroscopic-microscopic model, we come now to the numerical calculations of the total collective potential entering Eq. (18) on a six-dimensional mesh of vibrational collective variables: $\{\alpha_{20}, \alpha_{22}, \alpha_{3\nu}, \nu = 0, 1, 2, 3\}$ for the ^{156}Gd nucleus.

The ranges of those variables defining the shape of nucleus in the intrinsic coordinate system as well as the corresponding mesh steps $\Delta\alpha_{\lambda\mu}$ are listed below:

$$\alpha_{20}\epsilon(-1.0; 1.0), \quad \Delta\alpha_{20} = 0.05$$
$$\alpha_{22}\epsilon(-0.5; 0.5), \quad \Delta\alpha_{22} = 0.05$$
$$\alpha_{30}\epsilon(-0.3; 0.3), \quad \Delta\alpha_{30} = 0.1$$
$$\alpha_{31}\epsilon(-0.3; 0.3), \quad \Delta\alpha_{31} = 0.1$$
$$\alpha_{32}\epsilon(-0.3; 0.3), \quad \Delta\alpha_{32} = 0.1$$
$$\alpha_{33}\epsilon(-0.3; 0.3), \quad \Delta\alpha_{33} = 0.1, \quad (56)$$

which gives the mesh of $41 \times 21 \times 7 \times 7 \times 7 \times 7 = 2\,067\,261$ points, describing various quadrupole-octupole nuclear shapes. In order to interpolate the potential-energy values in an arbitrary point within this mesh, we use an efficient and fast approximation algorithm, based on the idea of the Strutinsky shell correction, described in Ref. [59].

Finally, let us consider the behavior of the macroscopic-microscopic potential energy function with regard to the action of the symmetrization group. The Woods-Saxon mean-field potential used to generate the single-particle spectra, by its particular construction, behaves in the same manner as the nuclear shape function $R(\vartheta, \varphi)$ of Eq. (4) under the symmetrization group operations $\bar{g} \in \bar{G}_s$. The same can be said about the liquid-drop energy which is finally determined through the functions of $R(\vartheta, \varphi)$ and the microscopic shell and pairing energy corrections depending only on set of mean-field eigenenergies. Concluding, the final macroscopic-microscopic potential energy as a function of the quadrupole-octupole deformation is invariant (scalar) with regard to the intrinsic symmetrization group $\bar{G}_s$. It means that no further modifications of the obtained through the presented method potential are necessary.

B. Potential energy surfaces

The two-dimensional cross sections of total macroscopic-microscopic potential energy surfaces (PES) are obtained by a projection of the full six-dimensional one onto demanded two-dimensional planes, assuming that the other four deformation parameters are fixed to zero. Figure 5 displays the total energy as function of the quadrupole (β, γ) deformation parameters which are directly connected with $(\alpha_{20}, \alpha_{22})$. There, the equilibrium energy minimum corresponding to quadrupole axial (prolate) shape of ^{156}Gd element is visible. The standard (β, γ) plots are very useful to trace the nonaxialities of quadrupole configurations. The $\gamma = 0$ gives the prolate (elongated) shape
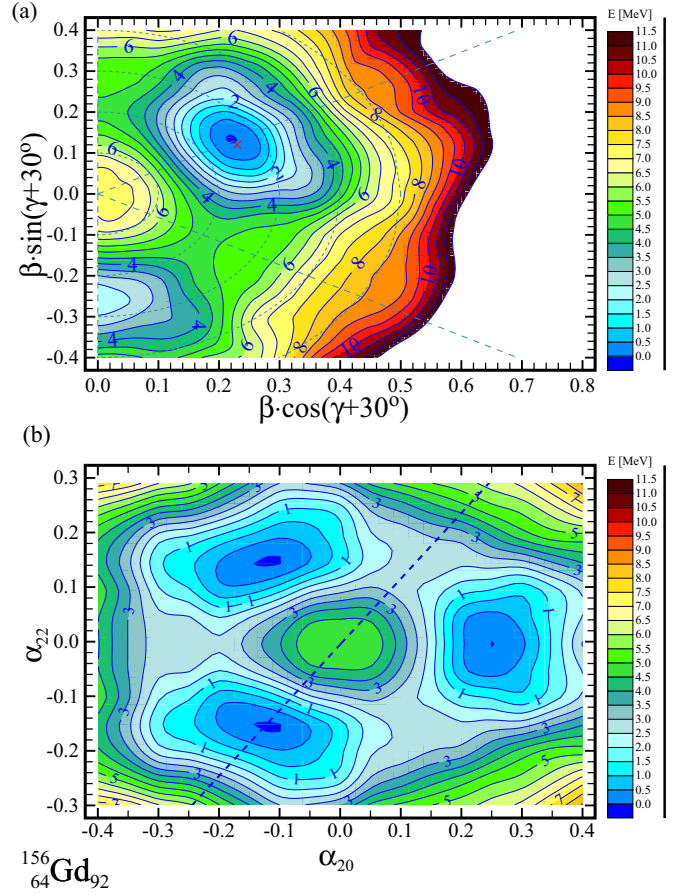

FIG. 5. The total energy of the ^{156}Gd in the quadrupole plane $(\beta\cos(\gamma + \pi/6), \beta\sin(\gamma + \pi/6))$ (a) and in $(\alpha_{20}, \alpha_{22})$ (b).

while $\gamma = \pm\pi/3$ allows us to have the oblate forms. For $\gamma \in (0, \pi/3)$ there is a space for triaxial shaped nuclei. This parametrization, however consistent and easy to read for quadrupole shapes, contains no room for higher multipolarity deformations discussed in the presented framework. We thus replot the upper figure in terms of exploited here $(\alpha_{20}, \alpha_{22})$ variables.

The straight dashed line in Fig. 5(a) indicates the axially symmetric shapes. The straight dashed line in the $(\alpha_{20}, \alpha_{22})$ [Fig. 5(b)] plane separates the shape configurations which are identical with respect to the $\bar{D}_4$ symmetrization group. Note that in the pure quadrupole shapes presented here, the true symmetrization group is, in fact, the octahedral $\bar{O}_h$ group containing $\bar{D}_4$ as its subgroup. In such a case, we observe the ground-state energy well occurring in the three $(\alpha_{20}, \alpha_{22})$ quadrupole configurations: the first for

$$\left(\alpha_{20}^{(gs)}, \alpha_{22}^{(gs)}\right) = (0.25, 0.0), \quad (57)$$

the second for

$$\alpha_{20}^{(2)} = \tfrac{1}{2}\left(-\alpha_{20}^{(gs)} + \sqrt{6}\alpha_{22}^{(gs)}\right),$$
$$\alpha_{22}^{(2)} = +\tfrac{1}{4}\left(\sqrt{6}\alpha_{20}^{(gs)} + 2\alpha_{22}^{(gs)}\right), \quad (58)$$

and the third for

$$\alpha_{20}^{(3)} = \tfrac{1}{2}\big(-\alpha_{20}^{(gs)} + \sqrt{6}\alpha_{22}^{(gs)}\big),$$
$$\alpha_{22}^{(3)} = -\tfrac{1}{4}\big(\sqrt{6}\alpha_{20}^{(gs)} + 2\alpha_{22}^{(gs)}\big). \qquad (59)$$

If, for any other than the ^{156}Gd nucleus, the ground state occurs for nonzero octupole deformations, then the symmetrization group turns to be a $\bar{D}_4$ group. Then, for

fixed $(\alpha_{20}^{(gs)}, \alpha_{22}^{(gs)})$ quadrupole deformation, the remaining four-dimensional full octupole domain can be split into the subdomains corresponding to identical shapes in the intrinsic frame. Assume that the point $(\alpha_{30}^{(0)}, \alpha_{31}^{(0)}, \alpha_{32}^{(0)}, \alpha_{33}^{(0)})$ describes a current octupole configuration. The identical shapes in the intrinsic frame (and rotated with respect to the laboratory one) correspond to the other seven points, say $(\alpha_{30}^{(i)}, \alpha_{31}^{(i)}, \alpha_{32}^{(i)}, \alpha_{33}^{(i)})$ for $i = 1, 2, \ldots, 7$ which can be obtained by applying the second property of Eq. (8) onto the point $(\alpha_{30}^{(0)}, \alpha_{31}^{(0)}, \alpha_{32}^{(0)}, \alpha_{33}^{(0)})$ [60],

$$\big(-\alpha_{30}^{(0)}, -\alpha_{31}^{(0)}, -\alpha_{32}^{(0)}, -\alpha_{33}^{(0)}\big), \big(\pm\alpha_{30}^{(0)}, \mp\alpha_{31}^{(0)}, \pm\alpha_{32}^{(0)}, \mp\alpha_{33}^{(0)}\big), \text{ for } i = 1, 2, 3;$$
$$\big(\pm\tfrac{1}{2}(\sqrt{5}\alpha_{33}^{(0)} - \sqrt{3}\alpha_{31}^{(0)}), \mp\tfrac{1}{4}(\sqrt{3}\alpha_{30}^{(0)} - \sqrt{10}\alpha_{32}^{(0)}), \pm\tfrac{1}{4}(\sqrt{6}\alpha_{33}^{(0)} + \sqrt{10}\alpha_{31}^{(0)}), \mp\tfrac{1}{4}(-\sqrt{6}\alpha_{32}^{(0)} - \sqrt{5}\alpha_{30}^{(0)})\big), \text{ for } i = 4, 5;$$
$$\big(\pm\tfrac{1}{2}(\sqrt{5}\alpha_{33}^{(0)} - \sqrt{3}\alpha_{31}^{(0)}), \pm\tfrac{1}{4}(\sqrt{3}\alpha_{30}^{(0)} - \sqrt{10}\alpha_{32}^{(0)}), \pm\tfrac{1}{4}(\sqrt{6}\alpha_{33}^{(0)} + \sqrt{10}\alpha_{31}^{(0)}), \pm\tfrac{1}{4}(-\sqrt{6}\alpha_{32}^{(0)} - \sqrt{5}\alpha_{30}^{(0)})\big), \text{ for } i = 6, 7. \quad (60)$$

Above, the points with a plus or minus sign correspond to two different transformed, four-dimensional octupole configurations. As seen from Eq. (60), for a fixed quadrupole deformations, a single octupole shape for all $\alpha_{3\mu}^{(0)} \neq 0$ can be obtained by using eight different deformation-parameter combinations. Within the $\bar{D}_4$ symmetrization group, each such shape can appear for the two (not three as in the case of an octahedral symmetrization group) different combinations of α_{20} and α_{22} described by (57) and (58). In total, the identical quadrupole-octupole shape should show up at maximum 16 times in the full (α_2, α_3) domain. The borders of subdomains of identical shapes in six-dimensional space can be found as a common part of all six linear conditions of the form

$$\alpha_{\lambda\mu}^{(i)}\big(\alpha_{20}^{(gs)}, \alpha_{22}^{(gs)}, \alpha_{30}^{(0)}, \alpha_{31}^{(0)}, \alpha_{32}^{(0)}, \alpha_{33}^{(0)}\big) = \alpha_{\lambda\mu}^{(0)} \qquad (61)$$

for $\lambda = \{2, 3\}$ and indices (i) as introduced in Eq. (60). One easily notices the property that a given transformed point $\alpha_{3\mu}^{(i)}$ in Eq. (60) depends only on the two, not, in general, on all four, values of $\alpha_{3\nu}^{(0)}$ and $\alpha_{3\nu'}^{(0)}$. This implies that the borders in question can be searched into the appropriate two-dimensional collective subspaces.

For examining the influence of the octupole degrees of freedom on the total potential energy, the maps presented in Fig. 6 may be useful. The projections of full PES on each available pair of octupole deformation parameters plotted there allow us to trace the structure of the equilibrium minimum and/or the depths and positions of possible local energy minima.

In Fig. 7 we show the total energy PES's as function of the quadrupole α_{20} and all octupole $\alpha_{3\mu}$ variables.

The total energy maps projected on the $(\alpha_{20}, \alpha_{3\mu})$ plane show slightly pronounced minima for negative α_{20} values. If, as seen in Fig. 6, there is no other than the ground-state well, which appears for octupoles $\alpha_{3\nu} = 0$, we should obtain by virtue of (58)–(60) exactly two additional "copies" of this minimum, both again for $\alpha_{3\nu} = 0$. In Fig. 7, these minima are slightly pronounced for $\alpha_{20} < 0$ and $\alpha_{22} = 0$. Their true position occurs roughly for $\alpha_{20}^{(2)} \approx -0.125$ and quite significant values of $\alpha_{22}^{(2)} \approx \pm0.153$ (note that Fig. 7 is done for $\alpha_{22}^{(2)} = 0.0$).

VIII. $B(E\lambda)$ PROBABILITIES

A numerical diagonalization of the collective Hamiltonian (18) represented in the basis of (38) provides us with realistic collective states. A certain subset of its eigenstates, with collective energies related to the ground state and the $B(E\lambda)$ values comparable to the experimental results, can be identified as the experimentally populated spectra, grouped into the bands of given spin, parity, etc. In the framework presented here we are focused mainly on investigating the ground-state band as well as the lowest negative-parity states in the ^{156}Gd nucleus. According to the experimental indications, the ground-state well in this nucleus is strongly quadrupole deformed with deformation $\beta = 0.34$. This means that in the equilibrium state octupole degrees of freedom are, in the first approximation, not excited. It implies that in the basis function (38) $\sum_{\rho=0}^{3} n_{3\rho} = 0$ while n_{20} and n_{22} values are admitted to be $\{0, 1, 2, 3\}$. For the negative-parity states, on the contrary, $n_{20} = 0$ and $n_{22} = 0$ while in the octupole part of this function, $\sum_{\rho=0}^{3} n_{3\rho} = \{1, 3\}$. Obviously, due to the parity reasons, even phonon numbers in the right-hand side of the previous condition are not allowed.

A separate problem is to fix the values of "shift" parameters $\alpha_{2\mu}^{\circ}$ and $\alpha_{3\nu}^{\circ}$ in Eq. (38) for $\lambda = \{2, 3\}$ and $-\lambda \geqslant \mu \leqslant \lambda$. These parameters make all the basis functions (38) are centered over the potential energy well where the minimum in our six-dimensional deformation space is in the point $(\alpha_{20}, \alpha_{22}, \alpha_{30}, \alpha_{31}, \alpha_{32}, \alpha_{33}) = (0.25, 0.0, 0.0, 0.0, 0.0, 0.0)$.

Now, we are ready to determine the last group of basis parameters in function (38), namely $\eta_{\lambda\mu}$. Certainly, for the incomplete basis set, comprising only several $(16 \div 24)$ different vibrational quadrupole-octupole configurations, the parameter $\eta_{\lambda\mu}$ introduced in Eq. (32), determining the interval of arguments, where the basis function differs substantially from zero is absolutely crucial. We have decided that the optimal values of those parameters should correspond to the minimal energy of the ground state, i.e.,

$$E_{gs} = E_{gs}(\{\eta_{\lambda\mu}\}) = \min. \qquad (62)$$

Within this work such a minimization is performed in successive steps. First, the true six-dimensional ground-state
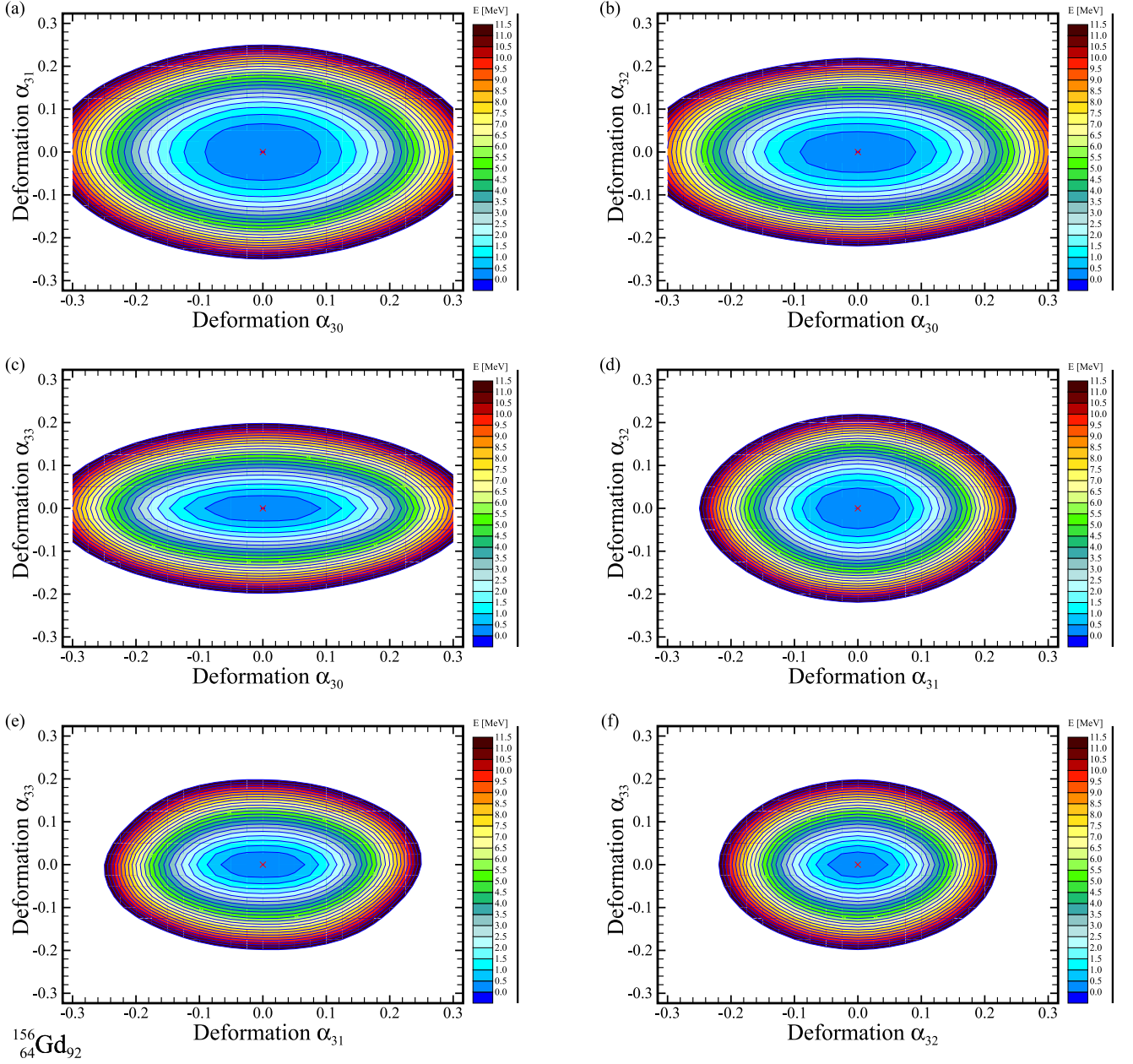
FIG. 6. The total energy of the ^{156}Gd in the octupole planes $(\alpha_{3\nu}, \alpha_{3\nu'})$, where axial symmetry is for $\mu = 0$ and nonaxial deformations are for $\{\mu, \nu\} = \{1, 2, 3\}$ for quadrupole deformation $\alpha_{20} = 0.25$ and $\alpha_{22} = 0.0$, being close to the ground-state deformation found in Fig. 7.

potential energy well is approximated within the least-squares method by the paraboloid potential of the harmonic oscillator of the form

$$V_{\text{osc}} = \frac{1}{2} \sum_{\lambda=2}^{3} \sum_{\mu=0}^{\lambda} g_{\mu\mu}^{(\lambda)} C_{\lambda\mu} (\alpha_{\lambda\mu} - \alpha_{\lambda\mu}^{\circ})^2, \quad \lambda = \{2, 3\}, \quad (63)$$

where $C_{\lambda\mu}$ plays a role of the potential energy stiffness parameter for the $(\lambda\mu)$ mode and $g_{\mu\mu}^{(\lambda)}$ is the metric tensor of our collective space. It is easy to check that for the harmonic oscillator the following relation is fulfilled:

$$\eta_{\lambda\mu}^{(0)} = (B_{\lambda\mu} C_{\lambda\mu})^{1/4}. \quad (64)$$

For simplicity, we have admitted that the mass $B_{\lambda\mu}$ corresponds to the mass-tensor value of Eq. (19) calculated in the ground state.

The shape of ^{156}Gd in the ground state is well α_{20} deformed, see Fig. 7. The one-dimensional energy profiles for the ground-state deformation $\alpha_{20} = 0.25$ and $\alpha_{22} = 0.0$, presented in Fig. 8, exhibit almost parabolic-like behavior as a function of axial and nonaxial octupole deformations for sufficiently low excitation energies of about 1–3 MeV. This feature allows for interpreting the octupole excitations in terms of phonon numbers of the oscillator basis functions (38). The potential towards α_{30} is flatter as compared to the ones for the other three octupole modes $\alpha_{3\mu}$. Hence, at first glance, it is the axial
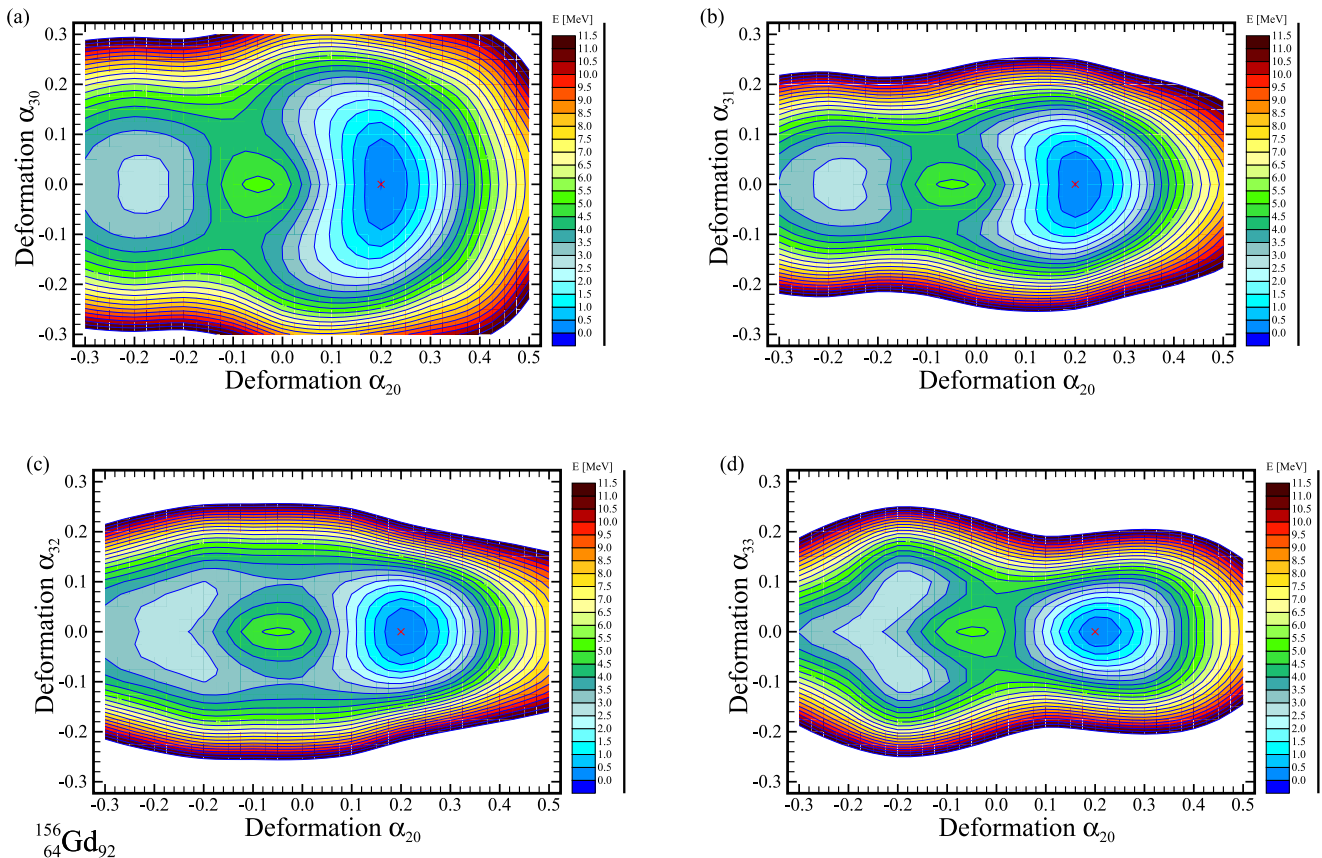
FIG. 7. The quadrupole ($\alpha_{20}, \alpha_{22} = 0$) versus octupole ($\alpha_{30}, \alpha_{31}, \alpha_{32}, \alpha_{33}$) energy maps.

octupole mode which seems to be most likely excited due to collective vibrations.

However, this statement is partially contradicted by the study of the relations between mass parameters B_{3030} and the other diagonal components $B_{3\mu3\mu}$. The values of the octupole mass tensor diagonal components are shown in Fig. 9. The procedure of obtaining the mass tensors has been discussed in Sec. IV at Eq. (19). The B_{3030} mass tensor has a minimum for $\alpha_{3\mu} = 0$ and weakly depends on axial octupole deformation. On average, its values are 2 times smaller than
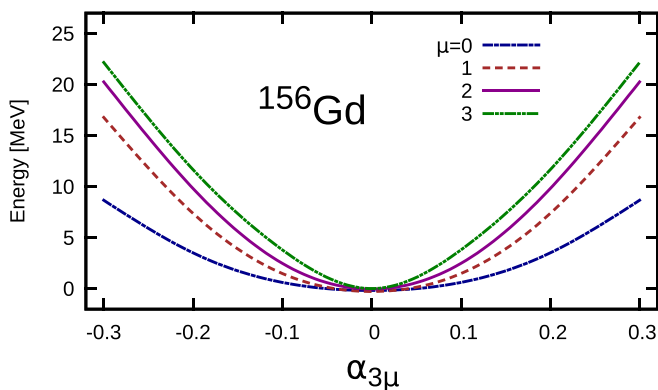
mass parameters calculated for nonaxial deformations in the vicinity of the ground-state minimum. The PES and mass parameters are the main factors governing the properties of the vibrational excitations in the nucleus.

As the second step, we determine the ratios $r_{\lambda\mu;\lambda0} \equiv \eta_{\lambda\mu}^{(0)}/\eta_{\lambda0}^{(0)}$. In an approximate way, varying only two, instead of six, parameters $\eta_{\lambda0}$ around $\eta_{\lambda0}^{(0)}$ values by a discrete step of $\Delta\eta_{\lambda0} = 0.5$, we can determine through condition (62), a demanded $\eta_{\lambda\mu}$ as $\eta_{\lambda\mu} = r_{\lambda\mu;\lambda0}\,\eta_{\lambda0}$, keeping, of course, the ratio $r_{\lambda\mu;\lambda0}$ untouched during the whole calculation.
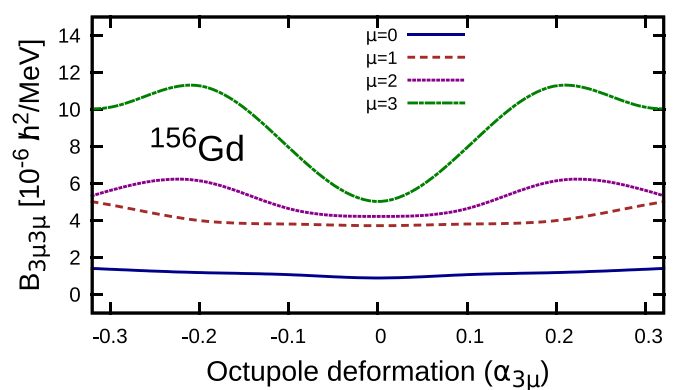

FIG. 8. The profiles of the total energy for the ground-state point of the ^{156}Gd nucleus with $\alpha_{20} = 0.25$ and $\alpha_{22} = 0.0$ as function of various octupole parameters: $\alpha_{30}, \alpha_{31}, \alpha_{32}, \alpha_{33}$.

FIG. 9. The profiles of the mass tensors for the ground-state point of the ^{156}Gd nucleus with $\alpha_{20} = 0.25$ and $\alpha_{22} = 0.0$ as a function of various octupole parameters: $\alpha_{30}, \alpha_{31}, \alpha_{32}, \alpha_{33}$.

The eigenstates of the Hamiltonian (18) calculated for the model parameters defined as written above can be used now to obtain the intraband and interband $B(E1)$ and $B(E2)$ transition probabilities and compared with the experimental data.

Now we come to the calculation of the electric reduced transition probabilities. As mentioned in Sec. II, an intrinsic coordinate system is chosen to fix the moment of inertia tensor of the quadrupole nuclear surface shape in the principal axes frame, i.e., $\alpha_{21} = \alpha_{2-1} = 0$ and $\alpha_{22} = \alpha_{2-2} \in \mathcal{R}$. The transformation of any irreducible tensor $\hat{T}_{\lambda\mu}$ from the intrinsic (intr) to laboratory (lab) frame obeys the relation (13). In the same way, we transform the collective electric transition operators [28]

$$\hat{Q}_{\lambda\mu}^{(\mathrm{lab})} = \sum_{\nu} D_{\mu\nu}^{\lambda}(\Omega)^{\star} \hat{Q}_{\lambda\nu}^{(\mathrm{intr})}. \quad (65)$$

Above, $\hat{Q}_{\lambda\nu}$ is the operator of the intrinsic electric multipole moment of the nucleus of A nucleons and Z protons which can be approximated, in the case of uniform proton density distribution of an effective radius $R_0 \approx 1.2\, A^{1/3}$, by

$$\hat{Q}_{\lambda\nu}^{(\mathrm{intr})} = \frac{3ZeR_0^{\lambda}}{4\pi} \left\{ \alpha_{\lambda\nu} + \frac{\lambda+2}{2\sqrt{4\pi}} \sum_{\lambda_1\lambda_2} \sqrt{\frac{(2\lambda_1+1)(2\lambda_2+1)}{2\lambda+1}} \right.$$
$$\left. \times (\lambda_1 0 \lambda_2 0 | \lambda 0) \left(\alpha_{\lambda_1} \otimes \alpha_{\lambda_2} \right)_{\nu}^{\lambda} \right\}. \quad (66)$$

Let us remember that Eq. (66) contains $\alpha_{\lambda\mu}$ variables which are, in general, complex. If one wants to calculate the matrix element of this operator between basis functions (38) defined in the space of real $\alpha_{\lambda\mu}$, where $\mu \geqslant 0$, the properties (2) and (3) should be applied. Finally, let us calculate the SO(3)-reduced matrix elements of the multipole transition operator between states (39) numbered by k and k' indices

$$\langle \Psi_{k';J'\kappa'\pi'} || Q_{\lambda}^{(\mathrm{lab})} || \Psi_{k;J\kappa\pi} \rangle$$
$$= \sum_{\mu} \langle \phi_{n'\pi'} | \hat{Q}_{\lambda\mu}^{(\mathrm{intr})} | \phi_{n\pi} \rangle \cdot \langle \tilde{R}_{\kappa'}^{J'} || D_{\cdot\mu}^{\lambda\star} || \tilde{R}_{\kappa}^{J} \rangle, \quad (67)$$

where J and J' are the angular momenta of the initial and final basis states, respectively. The symbol $\cdot\mu$ as the subscript by the Wigner function denotes that the considered reduced matrix element has been already reduced, using the Wigner-Eckart theorem, with respect to the first index. As easily seen, the expression $\langle \phi_{n'\pi'} | \hat{Q}_{\lambda\mu} | \phi_{n\pi} \rangle$ is simply the matrix element of the $\hat{Q}_{\lambda\mu}^{(\mathrm{intr})}$ intrinsic multipole moment operator of the charge distribution between vibrational part of the basis state (39). In this work, the latter is calculated numerically. The second element in Eq. (67) between the rotational functions can be evaluated analytically, using the standard Wigner-Eckart theorem, similarly as in Eq. (29),

$$\langle \tilde{R}_{\kappa'}^{J'} || D_{\cdot\mu}^{\lambda\star} || \tilde{R}_{\kappa}^{J} \rangle = \sqrt{(2J+1)} \sum_{KK'} \sum_{gg' \in \bar{G}_s} \left[\frac{1}{\mathrm{card}(\bar{G}_s)} \right]^2$$
$$\cdot \left[D_{\kappa'K'}^{J'}(g') \right]^{\star} D_{\kappa K}^{J}(g) (JK\lambda\mu | J'K'), \quad (68)$$

where for the symmetrization group $\bar{G}_s = \bar{D}_4$ and $\mathrm{card}(\bar{D}_4) = 8$.

To obtain the transitional matrix elements between a pair of full Hamiltonian eigenstates $|\Phi(J\pi)\rangle$ (or simply collective states), the matrix elements (67) between given $\langle$bra$|$ and $|$ket$\rangle$ basis functions should be first multiplied by the appropriate products of the two probability amplitudes corresponding to the k and k' indices (if necessary, for the "bra" function it is complex conjugated) and, second, doubly summed over the full basis set (k and k' indices). The probability amplitudes in question corresponding, e.g., to the mth Hamiltonian eigensolution are usually stored in the mth column (less often the row) of the orthonormal matrix of eigenvectors returned by the diagonalization routine.

Having obtained the transitional matrix element for the pair of full collective states according to the above prescription, the reduced transition probability of the electric $E\lambda$ transition finally reads

$$B(E\lambda, J \to J') = \frac{\left| \langle \Phi_{J'\pi'} || Q_{\lambda}^{(\mathrm{lab})} || \Phi_{J\pi} \rangle \right|^2}{2J+1}. \quad (69)$$

IX. RESULTS

In the presented framework we are able to estimate the positive- and negative-parity collective states of a nucleus and calculate the electric transitions between them as well. We performed calculations for ^{156}Gd nucleus which has been recently investigated, e.g., in Ref. [61,62] to search for the traces of the high rank symmetries (tetrahedral, octahedral) of its geometrical form. The purpose of this work is to construct, at least in an approximate way, a basic model enabling us to discuss the problem of a full set of octupole degrees of freedom and the interplays between them in this nucleus. Certainly, the model permits us to treat other nuclei with static, octupole-deformed stable configurations. This, we hope, will chart a path to develop more and more involved collective models to more closely approach the experimental results in the future.

A. Band structures

Analyzing the calculated and experimental values of the intraband and interband electric-transition probabilities, we can identify, with a significant dose of probability, the eigenstates which may correspond to states populated in the experiment. On the other hand, with regard to the observables such as the $B(E1)$, $B(E2)$ probabilities, energies of emitted photons, E_{γ}, which can be directly compared with the experimental data, we are able to construct, at most, three reasonable schemes of the ground state and the accompanying low-energy negative-parity rotational bands in ^{156}Gd. Each of those schemes corresponds to the experimental level scheme of Ref. [61,62] and reflects a possible scenario where the dominating octupole one-phonon excitation of $\alpha_{3\mu}$ type is considered as the bandhead of the lowest negative-parity band.

As often done, each Hamiltonian eigensolution is the linear combination of the orthonormal basis states with the corresponding amplitudes determined through the diagonalization of the Hamiltonian matrix. Analyzing those amplitudes, particularly in a given low-energy octupole, negative-parity state, one would be able to extract the dominating vibrational
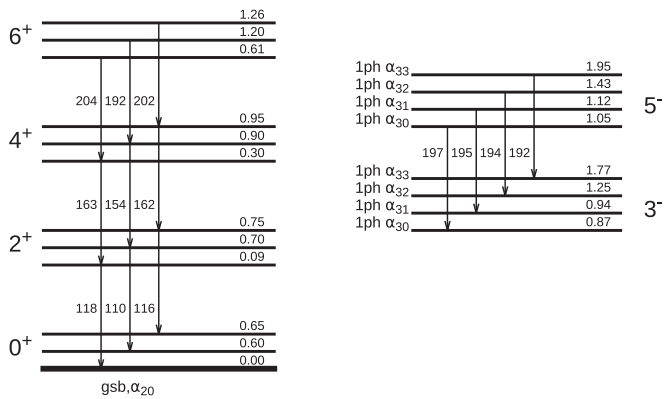
FIG. 10. The schematic presentation of the calculated levels for ^{156}Gd. The odd- and even-spin bands are drawn. There are a series of levels corresponding to every spin. The energies (in MeV) of each level are marked as well as the $B(E2)$ transition probabilities (in W.u.).

TABLE I. The γ-ray energies predicted theoretically (E_γ^{th}) and measured experimentally (E_γ^{exp}) in ILL Grenoble on ^{156}Gd [61,62]. Both even- and odd-spin bands are compared. The experimental values of the negative-parity bandhead is $(3_1^-) = 1.27$ MeV. The energies of the bandheads of the negative-parity states characterized by various types of the one-phonon octupole excitations are also shown.

Transition	E_γ^{th}	E_γ^{exp}
$(2^+ \rightarrow 0^+)$	90 keV	88 keV
$(4^+ \rightarrow 2^+)$	210 keV	199 keV
$(5^- \rightarrow 3^-)$	180 keV	130 keV
(3_0^-)	0.87 MeV	
(3_1^-)	0.94 MeV	
(3_2^-)	1.25 MeV	1.27 MeV
(3_3^-)	1.77 MeV	

mode and associated with this the symmetry of the considered configuration. Note that we are mainly interested in one-phonon vibrational excitations of axial, tetrahedral, or nonaxial type.

As we remember, the minimum of the octupole part of the potential energy well corresponding to the ground state appears for deformations $\alpha_{3\mu} = 0$ for all $\mu = \{0,1,2,3\}$. For such an octupole configuration, the negative-parity basis functions (38) are obtained solely with the use of the odd-order Hermite polynomials of octupole variables. As the outcome of calculations, the octupole excitations corresponding to a given $\alpha_{3\nu}$ mode are either of one- or three-phonon type. The latter lie much higher (some 2 MeV) in energy than the one-phonon excitations and are not considered in this work. We also observe that the individual one-phonon eigensolution contains hardly a minor admixture of the three-phonon component of the same multipolarity. Its magnitude is on the level of $5 \div 15\%$, depending on the state and thus contributes to the full state only insignificantly. This may indicate that the harmonic approach for low-energy octupole modes is rapidly convergent in this nucleus. Note also that the approximation formula used to generate the collective potential between the mesh points has nothing to do with any parabolic-like interpolation methods.

Figure 10 presents the most intensive of the obtained in current calculations $E2$ transitions within quadrupole and octupole bands. Apart from the quadrupole band built on the lowest quadrupole excitation, one can also distinguish two additional rotational bands, based on vibrational structures that are higher by 600 keV and 650 keV. Both of them are characterized by $B(E2)$ values of the order of 120 W.u.

In the negative-parity regime, the lowest two 3^- states in Fig. 10 are described by one-phonon excitations in the α_{30} and α_{31} modes, but the latter lies only some 70 keV higher. The so-called *tetrahedral* mode, described here by a real α_{32} variable, is placed more or less 380 keV higher than the lowest axial mode while the nonaxial one, characterized by α_{33} deformation, is placed some 900 keV above the lowest one. The latter therefore seems to be less likely excited. The same order of octupole modes is conserved for 5^- bundle of states.

As we observe, within the range of 0.5 MeV we can find three types of one-phonon octupole excitations that can potentially be treated as the bandheads of the lowest negative-parity odd-spin model bands. What is important, the $B(E2,5^- \rightarrow 3^-)$ probabilities between rotational states, based on each of those four excitations, are all around 200 W.u. The comparison of the present calculation results with experimental deexcitation energies is shown in Table I.

Now let us present some features of the positive-parity states. For every even-spin value available in the model, i.e., $J = 0,2,4,6$, we can distinguish three different vibrational structures which are responsible for producing strong quadrupole transitions, e.g., $B(E2,2^+ \rightarrow 0^+)$ being $110 \div 118$ W.u. Theoretically, those states can be considered as a potential band-heads for construction of three ground-state model bands. They differ by the structure of the quadrupole excitations. The lowest-energy state is in about 98% dominated by the zero-phonon $(u_0(\alpha_{20})u_0(\alpha_{22}))$ quadrupole oscillator solution. The other two are composed mainly of the one-phonon states of α_{20} and α_{22} modes with small 2-, 3-, . . . ,6-phonon admixtures. As mentioned, their energies with respect to the lowest 0^+ state are, respectively, 600 keV and 650 keV.

B. Calculated electric transitions

Let us now discuss the $B(E\lambda)$ transition probabilities obtained for different model bands. If the ground-state band is concerned, all the interband $B(E2)$ probabilities reproduced within this model are too small as compared to experimental measurements. In fact, the theoretical equilibrium static quadrupole deformation $\beta_2^{(\text{gs})} = 0.25$, which is the main factor determining the value of the transitional matrix element (67) is too small as compared to the experimental value of $\beta_2^{(\text{exp})} = 0.34$.

However, since $\beta_2^{(\text{exp})}$ describes a kind of *dynamical* deformation effect caused by the zero-point vibrations of the ground-state configuration, it is clear that its direct comparison with the static deformation of the mean-field potential-energy minimum is not that direct. According to our earlier estimates, the dynamical effects in question can

TABLE II. The predicted (Theory) and measured (Exp.) $E2$ transition probabilities for positive- and negative-parity bands. The mode of octupole excitation is also shown (Excitation). The experiment was done in ILL Grenoble for ^{156}Gd [61,62].

Transition	B(E2) (W.u.)		Dominating
$I_i^\pi \rightarrow I_j^\pi$	Theory	Exp.	Excitation
$2^+ \rightarrow 0^+$	118	187(5)	
$4^+ \rightarrow 2^+$	163	263(5)	
$5_0^- \rightarrow 3_0^-$	197	293^{+61}_{-134}	$\alpha_{30} \rightarrow \alpha_{30}$
$5_1^- \rightarrow 3_1^-$	195		$\alpha_{31} \rightarrow \alpha_{31}$
$5_2^- \rightarrow 3_2^-$	194		$\alpha_{32} \rightarrow \alpha_{32}$
$5_3^- \rightarrow 3_3^-$	191		$\alpha_{33} \rightarrow \alpha_{33}$

enlarge the static deformation of the ground state even by 20%. Nevertheless, by the fact that the rotational and vibrational motions are totally decoupled in this model, the obtained ratio of $B(E2,4^+ \rightarrow 2^+)/B(E2,2^+ \rightarrow 0^+) \approx 1.4$ agrees with the experimental issue, which is characteristic for electric transitions within fixed vibrational structure.

Comparing the $B(E2)$ results with those of Ref. [12] obtained through one of the recent version of the Bohr-Hamiltonian model, we see that for nuclei lighter than hafnium isotopes, the discrepancy of experimental and theoretical $B(E2)'$s exceeds 50 W.u. with the tendency to growing up.

Within the negative-parity model bands mentioned in the previous subsection, the strongest intraband $B(E2,5^- \rightarrow 3^-)$ transition probabilities are all of the order of 200 W.u. They are mainly contributed by the sole quadrupole part $u_0(\alpha_{20} - \alpha_{20}^\circ)\,u_0(\alpha_{22} - \alpha_{22}^\circ)$, common for all negative-parity basis states (38). Only a few Weisskopf units contributing to this value comes from pure octupole partly due to the fact that

the $E2$ transition operators (66) in the octupole part occur as the second-order couplings of the octupole variables only.

Now, the argument shifts α_{20}° and α_{22}° describe the position of the main octupole potential energy minimum on the quadrupole $(\alpha_{20}, \alpha_{22})$ plane. Note that in the ^{156}Gd nucleus, the only octupole minimum appears for all $\alpha_{3\nu} = 0$ and is "based" on the quadrupole ground-state well. Therefore, we admit that $\alpha_{20}^\circ = 0.25$ and $\alpha_{22}^\circ = 0$.

This value of reduced probability for the negative-parity band agrees with the experimental measurement within quite high error bars (see Table II). The energy E_γ in this transition stays in good agreement with the experimental value and is equal to 130 keV. The other series of obtained $B(E2, 5^- \rightarrow 3^-)$'s, of the order of 130 W.u., 65 W.u., and 15 W.u., are beyond the error bars.

We realize that the values of the $B(E2)$ transitions within the bands of interest are reproduced with unsatisfactory accuracy. Particularly, the $B(E2)$'s in the ground-state band are much beyond the experimental confidence interval. As a result, the quadrupole transition in the octupole band based on the quadrupole ground state, however, fits the interval between the error bars and is far from the reference value equal to 293 W.u.

As the next step, we calculate the interband $B(E1)$ transitions between the ground-state and the octupole, negative-parity model bands. Since the dipole $E1$ transitions are sensitive for the structures of both the positive- and negative-parity states, we expect the $B(E1)$ probabilities to be calculated with an order-of-magnitude accuracy. The dipole transitions allow us to finally eliminate the scenarios with the interband $B(E1)$ probabilities differing within more than one order of magnitude from the experimental data. Figure 10 visualizes the three modes of the positive-parity bands as well as the same number of selected negative-parity ones obtained in our
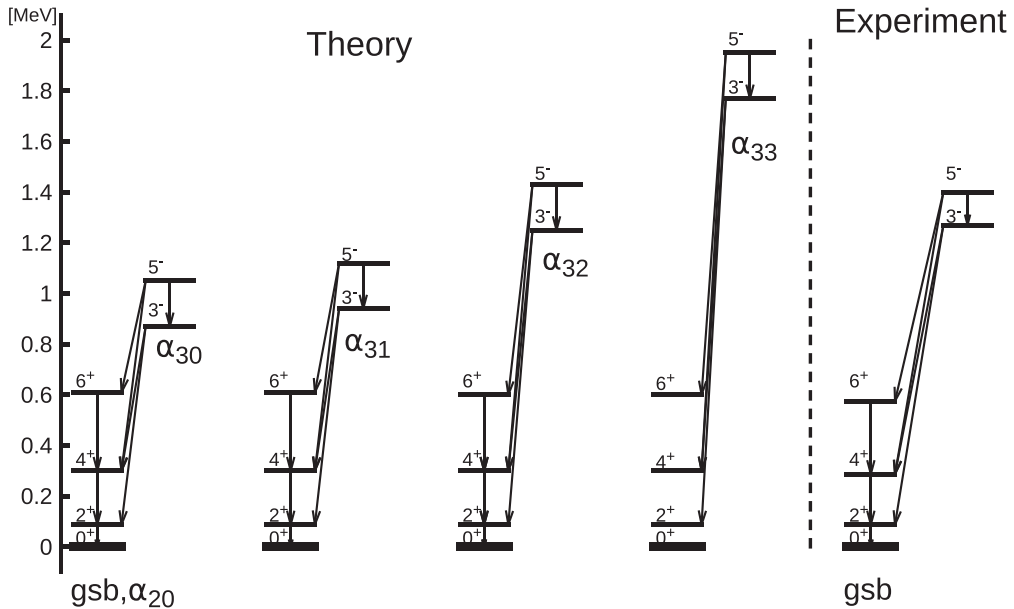

FIG. 11. The energy scale for the four model bands deduced from the presented calculations. The experimentally measured band is also shown.

TABLE III. The predicted and measured (Exp.) $E1$ transition probabilities between positive- and negative-parity bands. Symbols $\alpha_{3\mu}$ specify the type of the model bandhead structures. The experiment has been done in ILL Grenoble for ^{156}Gd [61,62].

Transition	Theory $B(E1)$ $(10^{-3}$W.u.)				
$I_i^\pi \to I_j^\pi$	α_{30}	α_{31}	α_{32}	α_{33}	Exp.
$3^- \to 2_1^+$	58	37	**0.36**	0.006	0.98(21)
$3^- \to 2_2^+$	0.052	0.053	1.5	4.3	
$3^- \to 2_3^+$	3.2	2.3	0.018	0.000001	
$3^- \to 4_1^+$	81	51	**0.51**	0.009	0.77(16)
$3^- \to 4_2^+$	0.082	0.14	2.2	6	
$3^- \to 4_3^+$	4.4	3.3	0.034	0.00001	
$5^- \to 4_1^+$	66	42	**0.41**	0.0072	$0.85^{+0.19}_{-0.38}$
$5^- \to 4_2^+$	0.67	0.12	1.8	5	
$5^- \to 4_3^+$	0.36	2.7	0.028	0.00008	
$5^- \to 6_1^+$	81	51	**0.53**	0.008	$0.64^{+0.14}_{-0.29}$
$5^- \to 6_2^+$	0.069	0.13	2.1	6.0	
$5^- \to 6_3^+$	4.5	3.2	0.023	0.0005	

calculations. In turn, Fig. 11 shows the transitions from all four negative-parity bands to the ground-state band.

The first model, illustrated in Fig. 11, assumes that the quadrupole band $(0^+,2^+,4^+,6^+)$ is composed of rotational states based on the third (energetically the highest) of selected in the previous section quadrupole structures, whereas the accompanying negative-parity band, $(3^-,5^-,\dots)$, is based on the one-phonon axial octupole (α_{30}) excitation. The best estimates of the $B(E1)$ probabilities given by this model are, on average, $4 \div 5$ times too large than the corresponding experimental values. Also, the energies of emitted photons, E_γ's, are here much too small compared to the experimental ones. In case the $E1$ transitions would finish in the two other energetically lower positive-parity states, the $B(E1)$ reduced probabilities become roughly either two orders of magnitude too large or two orders too small, respectively. The photon energies for this choice are getting closer to the experimental values.

The second scenario, shown in Fig. 11, where the ground-state band is assumed to be the same as in the previous scheme and the rotational band is built on the one-phonon α_{31} excitation, gives somewhat better estimates of $B(E1)$ probabilities, which are still about 3 times too high than in the experiment. The behavior of E_γ's is similar as in the first scheme. Again, if the final states in the ground-state band would be based on the two energetically lower bandheads, the corresponding $B(E1)$ values are, similarly as in the first scenario, not acceptable, regardless of the fact that now the E_γ's better fit the experimental values.

The third theoretical level scheme in this figure has, as the favorable positive-parity bandhead, the energetically lowest quadrupole structure, whereas the negative-parity band is constructed on the one-phonon *tetrahedral* (α_{32}) excitation. This scenario reproduces within the error bars the two of four measured experimental $B(E1)$ values. The $B(E1,5^- \to 4_1^+)$ transition is slightly out of the confidence interval while the

$B(E1,3^- \to 2_1^+)$ one is too small by a factor of two. The E_γ's of this scenario are reproduced in quite a satisfactory way, see Table III.

Comparing above three model bands, we can observe that the third model, based on the tetrahedral excitation, reproduces both the transition probabilities and the energies of emitted γ rays with acceptable accuracy.

X. SUMMARY AND PERSPECTIVES

We have constructed the collective model in the intrinsic frame based on the realistic collective Hamiltonian. Having diagonalized this Hamiltonian for the ^{156}Gd nucleus, one can then determine the reduced transition probabilities $B(E\lambda)$ within or between the model bands as well as the corresponding energies of emitted photons, E_γ's. The presented model treats all the quadrupole and octupole degrees of freedom on the same footing.

The Hamiltonian is diagonalized in a six-dimensional uncoupled harmonic oscillator basis. This basis is restricted to 0-, 1-, 2-, 3-phonon states in both the quadrupole and octupole parts.

Since only real parts of complex $\alpha_{\lambda\mu}$ collective variables are considered, the symmetrization group of our model is no longer the octahedral group $\bar{O}_h$, as for purely quadrupole vibrations, but rather its subgroup, $\bar{D}_4$.

The symmetry conditions discussed above forced us to use the generalized rotor Hamiltonian, which is a much more involved approximation than the standard nonaxial rotor. In return, we get the rotational Hamiltonian of required symmetry, where the coupling constants of "higher-order" terms, playing a role of perturbations to the standard rotor, can be fitted to a selected fragment of the full experimental rotational spectrum.

The calculated intraband $B(E2,6^+ \to 4^+)$, $B(E2,4^+ \to 2^+)$, $B(E2,2^+ \to 0^+)$, and $B(E2,5^- \to 3^-)$ reduced probabilities are systematically too small compared to the experimental data. In turn, the interband dipole $B(E1)$ probabilities, using the quadrupole-octupole-induced coupling $\alpha_{1\mu}$ dipole variables in the transition operator, are reproduced with accuracy up to an order of magnitude.

As discussed above, there appears to be a need to search for a more realistic model to determine the collective potential. The macroscopic-microscopic approximation used here gives quadrupole equilibrium deformations that are too small, which directly influence the $E2$ transitional matrix elements in both types of bands discussed. A promising solution would be to use a fully microscopic approach with a realistic nucleon-nucleon effective interaction that is able to generate the results within a reasonable "computer power" and time scale.

Surprisingly, the nonaxial α_{31} octupole mode is very close in energy to the axial α_{30} one, which, since the beginning, has supposed to have been the lowest. Studying only the potential-energy surfaces, the nonaxial modes have not been seriously taken into account as being able to efficiently compete with the axial mode. Of course, for a given basis cutoff criterion, such effects difficult to predict are the outcome of the interplay between complicated behavior of the potential-energy function and deformation-dependent

quadrupole and octupole mass tensors. The interesting features of the so-called tetrahedral states point out that all four octupole degrees of freedom are important to understand a complex behavior of negative-parity bands.

As also shown, in the presented approach the octupole three-phonon basis functions contribute only within several percentages to the leading one-phonon components. It confirms that the consideration of five, seven, or higher phonon components would have only a minor influence on the results presented.

The problem of quadrupole-octupole coupling by the one-diagonal components of one, common for quadrupole and octupole mass tensors in the kinetic-energy term, should also be considered in a future version of the presented model. We are also aware of the fact that for nuclei with "soft" potential-energy wells the coupling of vibrational and rotational modes should be switched on to provide us with more adequate description of collective states and electromagnetic transitions.

For the future applications it would be interesting to see what the present approach predicts in the case of, e.g., the ^{224}Ra nucleus, where static octupole deformation has been detected [63], as well as in neighboring nuclei currently under experimental investigation as possible candidates for stable octupole deformation. For ^{224}Ra, predictions of $B(E1)$, $B(E2)$, and $B(E3)$ probabilities by models of Refs. [64,65] at or close to the axial symmetry have been found to provide good results.

An open problem is the even-spin negative-parity spectra, recently measured in the ^{156}Gd nucleus. If the appropriate preliminary experimental data are confirmed, then we hope that the forthcoming work will be (partly) devoted to this topic.

In addition, to catch more subtle effects of the octupole vibrations, the density of the potential-energy mesh should be enlarged.

[1] P. A. Butler and W. Nazarewicz, Rev. Mod. Phys. **68**, 349 (1996).

[2] S. G. Rohoziński, Rep. Prog. Phys. **51**, 541 (1988).

[3] N. Minkov and P. M. Walker, Eur. Phys. J. A **48**, 80 (2012); Phys. Scr. **89**, 054021 (2014); Phys. Lett. B **694**, 119 (2010).

[4] L. Bonneau, N. Minkov, Dao Duy Duc, P. Quentin, and J. Bartel, Phys. Rev. C **91**, 054307 (2015).

[5] S. G. Rohoziński, Phys. Rev. C **56**, 165 (1997).

[6] J. Dudek, A. Góźdź, and N. Schunck, Acta Phys. Pol. B **34**, 2491 (2003).

[7] J. Dudek, A. Góźdź, N. Schunck, and M. Miśkiewicz, Phys. Rev. Lett. **88**, 252502 (2002).

[8] J. Dudek, J. Dobaczewski, N. Dubray, A. Góźdź, V. Pangon, and N. Schunck, Int. J. Mod. Phys. E **16**, 516 (2007).

[9] J. Dudek, A. Góźdź, D. Curien, V. Pangon, and N. Schunck, Acta Phys. Pol. B **38**, 1389 (2007).

[10] W. Nazarewicz, P. Olanders, I. Ragnarsson, J. Dudek, G. A. Leander, P. Möller, and E. Ruchowska, Nucl. Phys. A **429**, 269 (1984).

[11] W. Nazarewicz, J. Dudek, R. Bengtsson, T. Bengtsson, and I. Ragnarsson, Nucl. Phys. A **435**, 397 (1985).

[12] L. Próchniak and S. G. Rohoziński, J. Phys. G: Nucl. Part. Phys. **36**, 123101 (2009).

[13] P. G. Bizzeti and A. M. Bizzeti-Sona, Phys. Rev. C **70**, 064319 (2004).

[14] P. G. Bizzeti and A. M. Bizzeti-Sona, Phys. Rev. C **77**, 024320 (2008).

[15] J. Engel and F. Iachello, Phys. Rev. Lett. **54**, 1126 (1985).

[16] J. Engel and F. Iachello, Nucl. Phys. A **472**, 61 (1987).

[17] D. Bonatsos, D. Lenis, N. Minkov, D. Petrellis, and P. Yotov, Phys. Rev. C **71**, 064309 (2005).

[18] T. M. Shneidman, G. G. Adamian, N. V. Antonenko, R. V. Jolos, and S.-G. Zhou, Phys. Rev. C **92**, 034302 (2015).

[19] S. Ćwiok, J. Dudek, W. Nazarewicz, J. Skalski, and T. Werner, Comput. Phys. Commun. **46**, 379 (1987).

[20] M. K. Pal, *Theory of Nuclear Structure* (Scientific and Academic Editions, New York, 1983), 1st ed.

[21] J. Q. Chen, J. Ping, and F. Wang, *Group Representation Theory for Physicists* (World Scientific, Singapore, 2002).

[22] A. Góźdź, A. Szulerecka, A. Dobrowolski, and J. Dudek, Int. J. Mod. Phys. E **20**, 199 (2011).

[23] W. J. Swiatecki, Phys. Rev. **104**, 993 (1956).

[24] S. Cohen and W. J. Swiatecki, Ann. Phys. (NY) **22**, 406 (1963).

[25] J. R. Nix, Ann. Phys. (NY) **41**, 52 (1967).

[26] J. F. Cornwell, *Group Theory in Physics*, Vol. 1 (Academic Press, New York, 1994).

[27] D. Varshalovich, A. Moskalev, and V. Khershonski, *Quantum Theory of Angular Momentum* (World Scientific, Singapore, 1988).

[28] J. M. Eisberg and W. Greiner, *Nuclear Models: Collective and Single Particle Phenomena* (North-Holland, Amsterdam, 1987).

[29] A. Góźdź, J. Dudek, and M. Miśkiewicz, Acta Phys. Pol. B **34**, 2123 (2003).

[30] A. Góźdź and A. Olszewski, Int. J. Mod. Phys. E **13**, 357 (2004).

[31] M. Miśkiewicz, A. Góźdź, and J. Dudek, Int. J. Mod. Phys. E **13**, 127 (2004).

[32] A. Góźdź, A. Dobrowolski, J. Dudek, and K. Mazurek, Int. J. Mod. Phys. E **19**, 621 (2010).

[33] A. Dobrowolski, A. Góźdź, and A. Szulerecka, Phys. Scr. **T154**, 014024 (2013).

[34] S. G. Rohoziński, M. Gajda, and W. Greiner, J. Phys. G: Nucl. Phys. **8**, 787 (1982).

[35] C. Wexler and G. G. Dussel, Phys. Rev. C **60**, 014305 (1999).

[36] D. R. Inglis, Phys. Rev. **96**, 1059 (1954); **103**, 1786 (1956); S. T. Balyaev, Nucl. Phys. **24**, 322 (1961).

[37] R. D. Woods and D. S. Saxon, Phys. Rev. **95**, 577 (1954).

[38] N. Dubray, Ph.D. thesis, Université de Louis Pasteur de Strasbourg, France, 2005.

[39] V. M. Strutinsky, Yad. Fiz. **3**, 614 (1966).

[40] V. M. Strutinsky, Nucl. Phys. A **95**, 420 (1967).

[41] V. M. Strutinsky, Nucl. Phys. A **122**, 1 (1968).

[42] D. R. Bes and Z. Szymanski, Nucl. Phys. **28**, 42 (1963).

[43] M. Bolstreli, E. O. Fiset, J. R. Nix, and J. L. Norton, Phys. Rev. C **5**, 1050 (1972).

[44] K. Pomorski and J. Dudek, Phys. Rev. C **67**, 044316 (2003).

[45] J. Dudek, K. Pomorski, N. Schunck, and N. Dubray, Eur. Phys. J. A **20**, 15 (2003).

[46] J. Dudek, A. Góźdź, and D. Rosły, Acta Phys. Pol. B **32**, 2625 (2001).

[47] F. W. Byron and R. W. Fuller, *Mathematics of Classical and Quantum Physics* (Dover, New York, 1970).

[48] P. Ring and P. Schuck, *The Nuclear Many-Body Problem* (Springer-Verlag, New York, 1980).

[49] P. Jachimowicz, M. Kowal, and J. Skalski, Phys. Rev. C **87**, 044308 (2013).

[50] J. Dudek, K. Mazurek, and B. Nerlo-Pomorska, Int. J. Mod. Phys. E **13**, 117 (2004).

[51] J. Dudek, K. Mazurek, and B. Nerlo-Pomorska, Acta Phys. Pol. B **35**, 1263 (2004).

[52] J. Dudek, K. Mazurek, and B. Nerlo-Pomorska, Int. J. Mod. Phys. E **14**, 383 (2005).

[53] K. Mazurek, J. Dudek, and B. Nerlo-Pomorska, Acta Phys. Pol. B **36**, 1355 (2005).

[54] K. Mazurek and J. Dudek, AIP Conf. Proc. **802**, 153 (2005).

[55] H. J. Krappe, J. R. Nix, and A. J. Sierk, Phys. Rev. C **20**, 992 (1979).

[56] A. J. Sierk, Phys. Rev. C **33**, 2039 (1986).

[57] J. Dudek, A. Majhofer, and J. Skalski, J. Phys. G **6**, 447 (1980).

[58] M. S. Antony, Nuclide Chart 2002, IReS, Strasbourg, France, Association Européenne contre les Leucodystrophies.

[59] K. Pomorski, Comput. Phys. Commun. **174**, 181 (2006).

[60] A. Szulerecka, A. Dobrowolski, and A. Góźdź, Phys. Scr. **89**, 054033 (2014).

[61] M. Sugawara, H. Kusakari, Y. Yoshizawa, H. Inoue, T. Morikawa, T. Shizuma, and J. Srebrny, Phys. Rev. C **83**, 064308 (2011).

[62] M. Jentschel, W. Urban, J. Krempel, D. Tonev, J. Dudek, D. Curien, B. Lauss, G. de Angelis, and P. Petkov, Phys. Rev. Lett. **104**, 222502 (2010).

[63] L. P. Gaffney *et al.*, Nature (London) **497**, 199 (2013).

[64] P. G. Bizzeti and A. M. Bizzeti-Sona, Phys. Rev. C **88**, 011305(R) (2013).

[65] D. Bonatsos, A. Martinou, N. Minkov, S. Karampagia, and D. Petrellis, Phys. Rev. C **91**, 054315 (2015).